

Ab-initio insights into the structural, elastic, bonding, and thermophysical properties of UH_x ($x = 1, 2, 3, 5, 6, 7, 8$) under pressure: possible relevance to high- T_c superconductivity

Md. Ashrafal Alam^{1,2}, F. Parvin², S. H. Naqib^{2*}

¹Department of Physics, Mawlana Bhashani Science and Technology University, Santosh, Tangail 1902, Bangladesh

²Department of Physics, University of Rajshahi, Rajshahi 6205, Bangladesh

*Corresponding author: Postal address: Department of Physics, University of Rajshahi, Rajshahi 6205, Bangladesh; Cell: +8801715049589; Email: salehnaqib@yahoo.com

Abstract

Binary uranium hydrides, UH_x ($x = 1, 2, 3, 5, 6, 7, 8$), with different crystal symmetries are potentially interesting compounds for high- T_c superconductivity and as hydrogen storage systems. In this work we have explored the structural, elastic, mechanical, bonding, and thermophysical properties of these systems under uniform pressure via density functional theory based computations. Most of the results disclosed in this work are novel. From the calculations of the cohesive energy and enthalpy of formation, we have found that the titled compounds are chemically stable. The computed elastic constants at different pressures ensure elastic stability. All the binary hydrides are mechanically anisotropic. Pressure induced brittle-ductile transition takes place under high pressure. The compounds are machinable with the cubic $\alpha\text{-UH}_3\text{-Pm-3n}$ showing very high value of the machinability index. All the compounds are fairly hard with cubic UH_8 showing superhard character. The Debye temperatures and acoustic velocities of these compounds are high; the highest value is found for the cubic UH_8 . The melting temperature, Grüneisen parameter, minimal phonon thermal conductivity, and the thermal expansion coefficient of these compounds have also been studied at different pressures. All these parameters show excellent correspondence with the estimated Debye temperature, elastic parameters and bonding characteristics.

Keywords: DFT calculations; Hydride superconductors; Effect of pressure; Elastic properties; Thermophysical properties

1. Introduction

In 1968 Ashcroft predicted theoretically high temperature superconductivity in solid metallic hydride [1]. From this prediction Sieverts et al. [2] reported UH_3 hydride. Later Driggs et al. [3]

and Mulford et al. [4] synthesized and identify UH_3 known as the $\alpha\text{-UH}_3$ compound. Recently some experimental and theoretical groups predicted several actinium hydrides such as UH_8 with high superconducting transition temperature 193 K [5]. Some example of recently reported binary hydrides with superconducting transition temperatures under pressure are: SiH_4 [6] ($T_c \sim 17$ K @ 96 GPa), H_3S [7, 8] ($T_c \sim 203$ K @ 155 GPa), AcH_5 [9] ($T_c \sim 79$ K @ 150 GPa), AcH_6 [9] ($T_c \sim 204$ K @ 200 GPa), AcH_{10} [9] ($T_c \sim 251$ K @ 200 GPa), ThH_9 [9] ($T_c \sim 146$ K @ 170 GPa), ThH_{10} [9] ($T_c \sim 161$ K @ 170 GPa). Besides experimentally realized and theoretically predicted superconductivity, actinide hydrides have important applications in the nuclear power plant as fuel material [5]. Among the actinide series, uranium is widely used as nuclear material. On the other hand, heated uranium reacts with hydrogen and produces uranium hydrides. The uranium-hydrogen binary system has attracted wide attention of scientific community due to its application in the fields of chemical hydrogen storage material and nuclear technology industry [10]. Uranium hydrides are also candidate of high superconducting temperature materials such as UH_8 ($T_c \sim 193$ K) [5, 11-15]. For these reasons, recently uranium hydrides have drawn significant attention of the scientific community. At high pressure some new binary uranium hydrides were predicted. Kruglov et al. [16] predicted a series of uranium hydrides such as UH , U_2H_3 , UH_2 , U_2H_5 , UH_3 , U_3H_{10} , UH_5 , UH_6 , U_2H_{13} , UH_7 , UH_8 , U_2H_{17} and UH_9 by using ab-initio evolutionary crystal structure prediction. Among of these uranium hydrides, only UH_7 , UH_8 and UH_9 have superconducting properties under pressure following theoretical predictions. Wang et al. [17], on the other hand, experimentally confirmed the existence of superconductivity in UH_5 , UH_7 and UH_8 under pressure. Souter et al. [18] and Raab et al. [19] investigated and reported results on uranium polyhydrides: UH , UH_2 , UH_3 and $\text{UH}_4(\text{H}_2)_n$ ($n = 0, 1, 2, 3, 4, 5, 6$).

Uranium hydrides are novel hydrogen-rich system which contains 5f electrons. Min Liu et al. [5] investigated structural, electronic, mechanical and magnetic properties on some uranium hydride systems. Kruglov et al. [16] predicted crystal structure and calculated T_c for UH_7 , UH_8 and UH_9 only for a particular pressure. The calculated values of T_c for UH_7 is 65.8 K and 56.7 K (@ 0 GPa), 54.1 K and 43.7 K (@ 20 GPa), for UH_8 it is 55.2 K and 46.2 K (@ 0 GPa), 33.3 K and 23.4 K (@ 50 GPa), and for UH_9 it is 31.2 K and 19.9 K (@ 300 GPa). Detailed pressure dependent studies of the physical properties of many of these uranium hydrides are still lacking. The superconducting state properties of phonon mediated systems are strongly dependent on the structural and thermophysical properties including the Debye temperature. To address these

issues we have selected the UH, UH₂, UH₃, UH₅, UH₆, UH₇, UH₈ binary uranium hydrides in this study. Pressure dependent structural, elastic, bonding and thermophysical properties of these compounds are studied in detail in this work employing density functional theory (DFT) based approach. The pressure ranges have been selected following previous studies [16]. Different structures belonging to the orthorhombic, cubic and hexagonal symmetry have been considered.

The subsequent sections of the work have been arranged as follows: Section 2 describes the methodology briefly. Section 3 contains computational results and discussion. Finally, in Section 4, conclusions are drawn.

2. Computational scheme

For geometry optimization of the compounds of interest, plane wave pseudopotential [20] method was used as implemented in the CASTEP code [21]. Generalized gradient approximation (GGA) with PBE functional [22] was used for the electronic exchange-correlation terms. Ultrasoft pseudopotential was used for the calculations of electron-ion interactions [23]. The BFGS algorithm was used to minimize the total energy and internal forces [24] within the optimized crystal structure. Monkhorst–Pack grid [25] was used for k -point sampling. The elastic constants were determined using the stress-strain module in CASTEP. Thermophysical parameters were computed from the elastic constants and moduli.

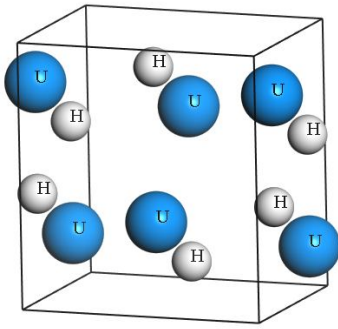
Convergence of tolerance parameters, energy cut-off and size of k -point grids of UH_{*x*} ($x = 1, 2, 3, 5, 6, 7, 8$) used for geometry optimizations were as follows:

Parameters	UH (<i>Cmcm</i>)	UH (<i>P6₃/mmc</i>)	UH ₂ (<i>Pbcm</i>)	α -UH ₃ (<i>Pm-3n</i>)	UH ₅ (<i>P6₃mc</i>)	UH ₆ (<i>P6₃/mmc</i>)	UH ₇ (<i>P6₃/mmc</i>)	UH ₈ (<i>Fm-3m</i>)
Quality	Ultra-fine	Ultra-fine	Ultra-fine	Ultra-fine	Ultra-fine	Ultra-fine	Ultra-fine	Ultra-fine
Energy (eV/atom)	5.0×10^{-6}	5.0×10^{-6}	5.0×10^{-6}	5.0×10^{-6}	5.0×10^{-6}	5.0×10^{-6}	5.0×10^{-6}	5.0×10^{-6}
Max. force (eV/Å)	0.01	0.01	0.01	0.01	0.01	0.01	0.01	0.01
Max. stress (GPa)	0.02	0.02	0.02	0.02	0.02	0.02	0.02	0.02
Max. displacement (Å)	5.0×10^{-4}	5.0×10^{-4}	5.0×10^{-4}	5.0×10^{-4}	5.0×10^{-4}	5.0×10^{-4}	5.0×10^{-4}	5.0×10^{-4}
Energy cut-off (eV)	550	550	550	450	550	550	550	550
k -points	13×12×17	16×16×15	7×8×11	22×22×22	10×10×6	15×15×10	15×15×9	18×18×18

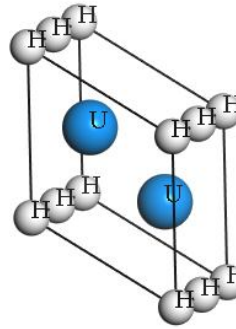
3. Results and analysis

3.1 Structure and stability

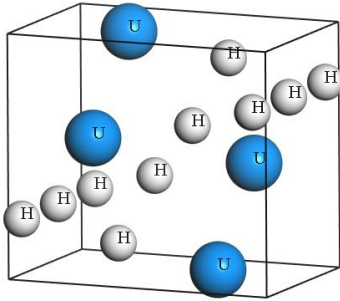
The different crystal structures of binary uranium hydrides UH_x ($x = 1, 2, 3, 5, 6, 7, 8$) are shown schematically in Fig. 1. The optimized unit cell parameters (a , b , c , and V), the cohesive energy E_{coh} , and the enthalpy of formation (ΔH) at different hydrostatic pressures for each structure are summarized in Table 1.



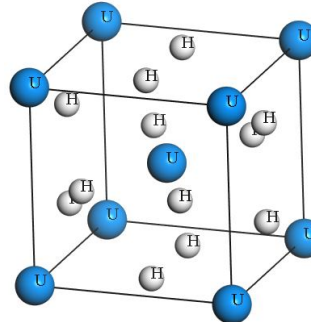
(a) UH-Cmcm



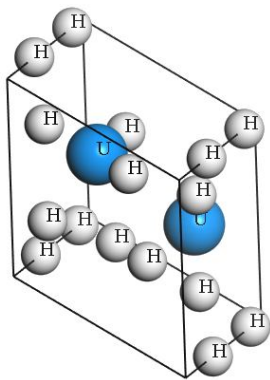
(b) $\text{UH-P6}_3/\text{mmc}$



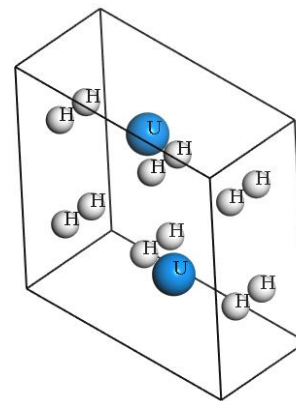
(c) $\text{UH}_2\text{-Pbcm}$



(d) $\alpha\text{-UH}_3\text{-Pm-3n}$



(e) $\text{UH}_5\text{-P6}_3\text{mc}$



(f) $\text{UH}_6\text{-P6}_3/\text{mmc}$

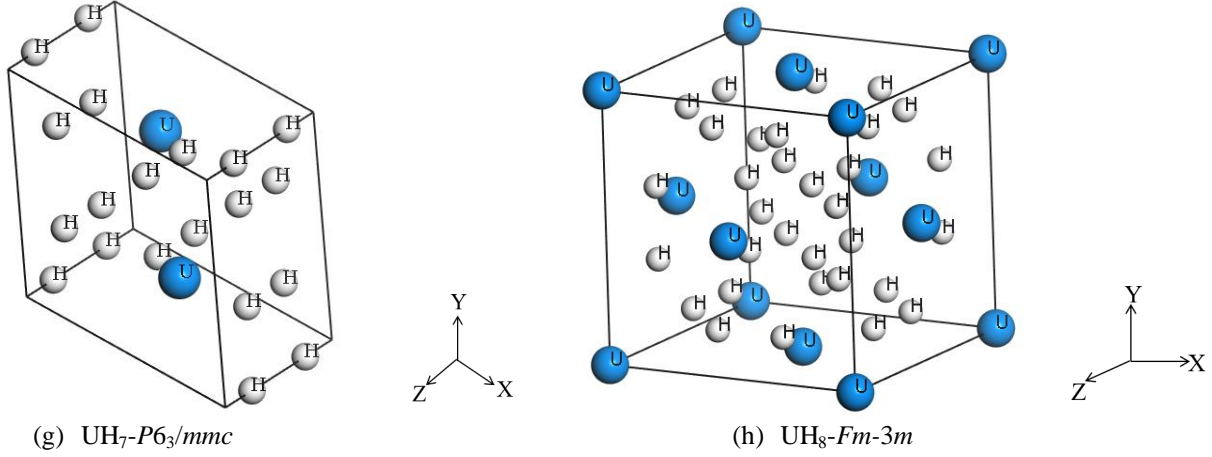


Figure 1: Schematic crystal structures of UH_x ($x = 1, 2, 3, 5, 6, 7, 8$) compounds in different symmetries.

UH-Cmcm , $\text{UH}_2\text{-Pbcm}$, and $\text{UH}_8\text{-Fm-3m}$ structures contain four formula units and $\text{UH-P6}_3/\text{mmc}$, $\alpha\text{-UH}_3\text{-Pm-3n}$, $\text{UH}_5\text{-P6}_3\text{mc}$, $\text{UH}_6\text{-P6}_3/\text{mmc}$ and $\text{UH}_7\text{-P6}_3/\text{mmc}$ structures contain two formula units in the unit cells. The computed values of the optimized lattice parameters are consistent with the previous results for all of the structures considered herein. In this work, we have calculated the cohesive energy per atom using the approach adopted in Refs. [26-28] for the first time, to determine the chemical stability. The E_{coh} has been computed using the following equation:

$$E_{\text{coh}} = \frac{x E_{\text{H}} + E_{\text{U}} - E_{\text{UH}_x}}{x + 1} \quad (1)$$

where, E_{UH_x} is total energy per formula unit of UH_x and E_{U} and E_{H} are the total energies of single U and H atom in the solid states, respectively, and x is the number of H atoms in formula. From Table 1, it is found that the values of cohesive energy per atom are positive, which indicate that all of the structures of UH_x ($x = 1, 2, 3, 5, 6, 7, 8$) are chemically stable.

Table 1. Structural properties of UH_x ($x = 1, 2, 3, 5, 6, 7, 8$) compounds under different pressures.

Compounds	Crystal System Space Group Space Group No.	Pressure, P (GPa)	Lattice parameters (Å)			Deviation (%) from earlier study [16]			Volume, V (Å ³)	Cohesive energy (eV/atom)	Enthalpy, (ΔH) (eV) $\times 10^3$
			a	b	c	a	b	c			
UH	Orthorhombic	20	4.73550	5.00747	3.58450				85.00	6.27	-5.66860
	<i>Cmcm</i>	30	4.64283	4.95360	3.54750	2.08	1.25	1.02	81.59	6.21	-5.66340
	63	30	4.63700	4.94500	3.54800					--	
		40	4.56404	4.90867	3.51432				78.73	6.13	-5.65840
UH	Hexagonal	55	3.50607	3.50607	3.39310				36.12	5.86	-2.82556
	$P6_3/mmc$	65	3.47707	3.47707	3.36195	-0.03	-0.03	0.03	35.20	5.78	-2.82333
	194	65	3.47800	3.47800	3.36100						
		75	3.45106	3.45106	3.33508				34.40	5.69	-2.82116
UH ₂	Orthorhombic	20	5.53594	4.90788	3.63823				98.85	5.40	-5.73136
	<i>Pbcm</i>	30	5.42330	4.86632	3.59109	0.47	-0.01	0.06	94.77	5.35	-5.72532
	57	30	5.39800	4.86700	3.58900						
		40	5.32447	4.83174	3.54986				91.33	5.29	-5.71952
α -UH ₃	Cubic	0	4.04861	4.04861	4.04861	-1.71	-1.71	-	66.36	5.02	-2.90452
	<i>Pm-3n</i>	0	4.11800	4.11800	4.11800						--
	223	10	3.95685	3.95685	3.95685				61.95	5.01	-2.90052
		20	3.88494	3.88494	3.88494				58.63	4.97	-2.89676
UH ₅	Hexagonal	10	3.75315	3.75315	5.90715				72.06	4.40	-2.96261
	$P6_3mc$	20	3.69378	3.69378	5.79482	-	-	-	68.47	4.37	-2.95823
	186	20	3.69500	3.69500	5.81600						--
		30	3.64546	3.64546	5.69702				65.57	4.33	-2.95405
UH ₆	Hexagonal	10	4.02046	4.02046	5.44992				76.29	4.21	-2.99338
	$P6_3/mmc$	20	3.94806	3.94806	5.37774	0.10	0.10	-	72.59	4.19	-2.98874
	194	20	3.94400	3.94400	5.38500						--
		30	3.89010	3.89010	5.31418				69.64	4.15	-2.98431
	Hexagonal	0	4.04069	4.04069	5.83566				82.51	4.04	-3.02874
UH ₇	$P6_3/mmc$	10	3.96083	3.96083	5.73643				77.94	4.03	-3.02374
	194	20	3.89809	3.89809	5.65426	0.10	0.10	0.16	74.41	4.01	-3.01899
		20	3.89400	3.89400	5.64500						--
		30	3.84427	3.84427	5.58619				71.49	3.98	-3.01444
		40	3.79888	3.79888	5.52278				69.02	3.95	-3.01006
UH ₈	Cubic	0	5.53373	5.53373	5.53373				169.45	3.85	-6.11670
	<i>Fm-3m</i>	30	5.27966	5.27966	5.27966				147.17	3.80	-6.08729
	225	40	5.22016	5.22016	5.22016				142.25	3.77	-6.08720
		50	5.16651	5.16651	5.16651	0.16	0.16	0.16	137.91	3.73	-6.06952
		50	5.15800	5.15800	5.15800						
		60	5.11837	5.11837	5.11837				134.09	3.70	-6.06103

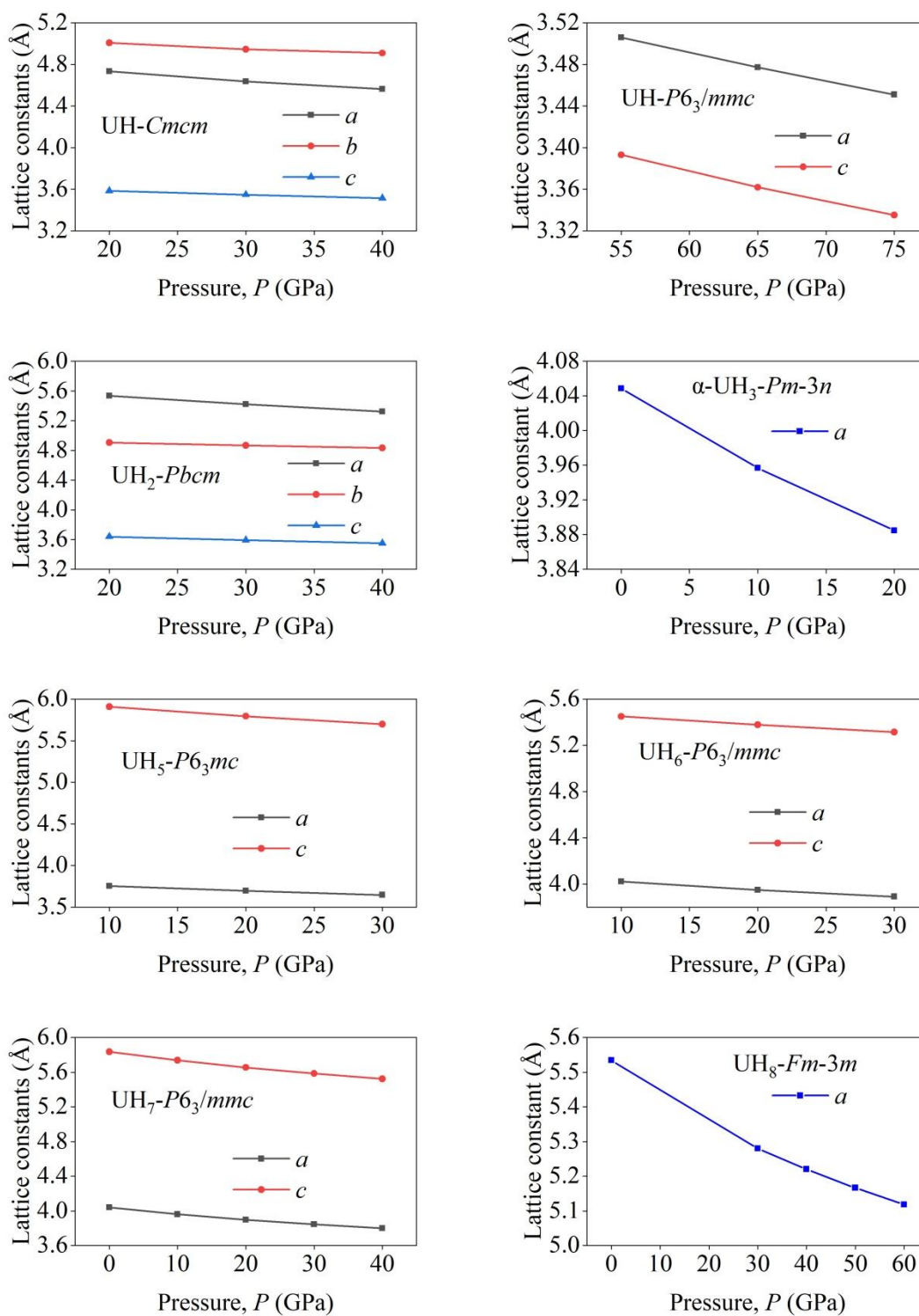


Figure 2: Lattice constants of UH_x ($x = 1, 2, 3, 5, 6, 7, 8$) compounds under pressure.

For all the compounds under consideration, the values of lattice parameters a , b and c decrease with pressure shown in [Table 1](#) (cf. [Fig. 2](#)). We do not see any abrupt change in the lattice parameters with, which indicates that the structures are stable in the pressure range considered. This is consistent with the predictions of earlier [[16](#), [17](#)]. Among the binaries, the cubic UH_8 - $Fm\bar{3}m$ structure shows the highest axial compressibility. This particular compound also has significantly larger unit cell volume.

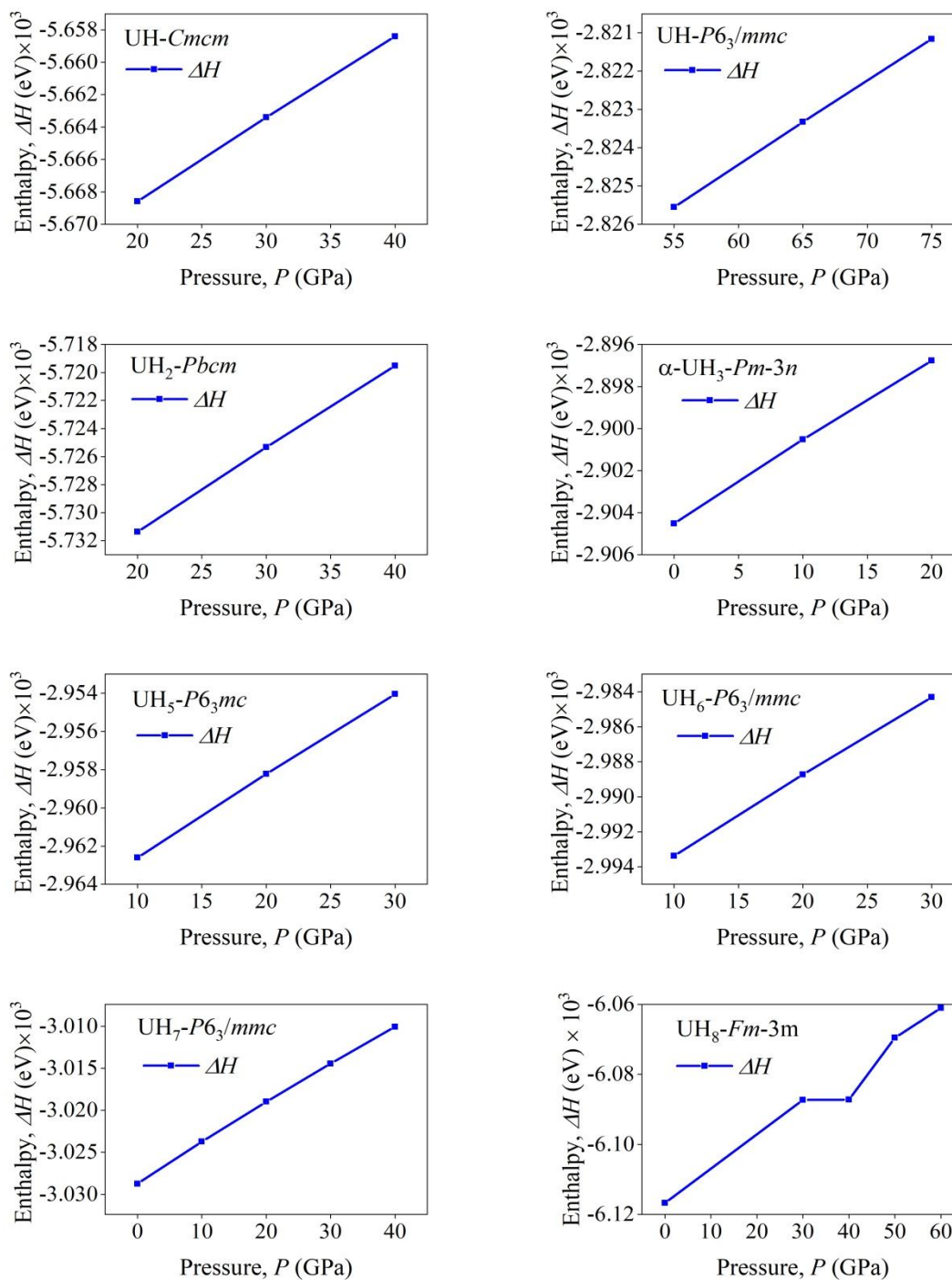


Figure 3: Enthalpy of formation of UH_x ($x = 1, 2, 3, 5, 6, 7, 8$) compounds under pressure.

The values of enthalpies of formation under pressure support the phase stability (cf. Fig. 3) of the UH_x ($x = 1, 2, 3, 5, 6, 7, 8$) compounds under different hydrostatic pressures. The increase in the enthalpy with increase in pressure is natural since both the internal energy and the product PV

increase with pressure for solids. The nonmonotonic behavior observed for cubic $\text{UH}_8\text{-Fm-}3m$ in the pressure range 30 GPa – 40 GPa implies that the conventional variations of the internal energy and the product PV are not maintained in this pressure interval. This may imply a change in the bonding features at these pressures.

3.2 Elastic properties

3.2.1 Single crystal elastic constants

For the orthorhombic crystal structure there are nine independent elastic constants: C_{11} , C_{22} , C_{33} , C_{44} , C_{55} , C_{66} , C_{12} , C_{13} and C_{23} . For hexagonal systems there are six elastic constants: C_{11} , C_{12} , C_{13} , C_{33} , C_{44} , and C_{66} . Except C_{66} , the other five are independent elastic constants in this case. For cubic crystal there are three independent elastic constants: C_{11} , C_{12} , and C_{44} . All of these elastic constants are tabulated in [Table 2](#) for the UH_x ($x = 1, 2, 3, 5, 6, 7, 8$) compounds at different pressures. From [Table 2](#), it is seen that C_{ij} increases almost linearly with pressure. All the computed values of C_{ij} are positive and all these parameters show monotonic variation with pressure indicating that there are no pressure induced structural modifications in the binary uranium hydrides under study for the pressure ranges considered. The values of C_{11} , C_{22} , and C_{33} represent along [100], [010] and [001] directional resistance against uniaxial stress, respectively. Greater values of C_{11} , C_{22} , and C_{33} indicate higher levels of incompressibility in the corresponding directions. From [Table 2](#), it is observed that UH-Cmcm has the highest incompressibility along [001] direction because $C_{33} > C_{22} > C_{11}$. $\text{UH-P6}_3\text{/mmc}$ has the highest incompressibility along [001] directions because $C_{33} > C_{22} = C_{11}$. $\text{UH}_2\text{-Pbcm}$ has highest incompressibility along [010] directions because $C_{22} > C_{33} > C_{11}$. For $\alpha\text{-UH}_3\text{-Pm-}3n$ incompressibility is the same along the three principle axes because cubic symmetry demands $C_{11} = C_{22} = C_{33}$. The most incompressible direction is [001] for $\text{UH}_5\text{-P6}_3\text{mc}$, $\text{UH}_6\text{-P6}_3\text{/mmc}$, and for $\text{UH}_7\text{-P6}_3\text{/mmc}$, it is [001] because $C_{33} > C_{22} = C_{11}$. The largest values of the elastic constants are found in the $\text{UH-P6}_3\text{/mmc}$ and $\text{UH}_8\text{-Fm-}3m$ structures indicating that directional deformation resistances are very strong in these two compounds. The elastic stability of the compounds can be judged from the values of C_{ij} .

Table 2. Calculated single crystal elastic constants C_{ij} (GPa) of UH_x ($x = 1, 2, 3, 5, 6, 7, 8$) compounds under different pressures.

Compounds	Crystal System Space Group Space Group No.	Pressure, P (GPa)	Single crystal elastic constants, C_{ij} (GPa)									Ref.
			C_{11}	C_{12}	C_{13}	C_{22}	C_{23}	C_{33}	C_{44}	C_{55}	C_{66}	
UH	Orthorhombic	20	357.75	110.19	87.80	460.21	188.42	527.39	201.28	87.15	87.67	
	<i>Cmcm</i>	30	413.51	142.09	101.22	524.19	222.31	600.52	222.68	94.81	92.19	[This]
	63	40	473.87	173.63	112.37	590.52	257.46	669.77	244.99	102.44	86.19	
UH	Hexagonal	55	743.91	276.35	112.24	743.91	112.24	812.60	123.25	123.25	233.78	
	<i>P6₃/mmc</i>	65	812.88	300.54	142.71	812.88	142.71	904.98	134.88	134.88	256.17	
	194	75	880.27	330.09	172.47	880.27	172.47	987.28	147.83	147.83	275.09	
UH ₂	Orthorhombic	20	348.35	136.33	90.70	506.76	165.57	456.25	170.51	76.45	73.35	
	<i>Pbcm</i>	30	385.88	158.77	107.21	575.02	201.71	522.22	199.70	71.70	84.34	[This]
	57	40	417.07	181.11	122.23	635.98	238.85	584.59	224.88	68.01	96.01	
α -UH ₃	Cubic	0	286.26	46.52	46.52	286.26	46.52	286.26	63.64	63.64	63.64	
	<i>Pm-3n</i>	10	351.56	71.07	71.07	351.56	71.07	351.56	55.43	55.43	55.43	[This]
	223	20	416.39	90.17	90.17	416.39	90.17	416.39	34.16	34.16	34.16	
UH ₅	Hexagonal	10	308.60	147.78	86.45	308.60	86.45	318.64	104.95	104.95	80.41	
	<i>P6₃mc</i>	20	369.73	177.98	115.12	369.73	115.12	364.82	109.93	109.93	95.88	[This]
	186	30	426.74	208.46	139.50	426.74	139.50	406.16	111.71	111.71	109.14	
UH ₆	Hexagonal	10	331.05	101.31	92.27	331.05	92.27	440.92	122.61	122.61	114.87	
	<i>P6₃/mmc</i>	20	387.06	131.48	119.13	387.06	119.13	498.68	134.33	134.33	127.79	[This]
	194	30	441.84	161.02	143.29	441.84	143.29	551.63	145.77	145.77	140.41	
UH ₇	Hexagonal	0	310.90	74.70	65.07	310.90	65.07	371.61	132.27	132.27	118.10	
	<i>P6₃/mmc</i>	10	375.24	100.36	91.26	375.24	91.26	431.00	151.96	151.96	137.44	
	194	20	438.75	125.07	118.36	438.75	118.36	489.23	167.80	167.80	156.84	[This]
		30	494.34	149.85	146.00	494.34	146.00	526.78	182.63	182.63	172.24	
		40	548.15	174.44	171.85	548.15	171.85	588.04	197.26	197.26	186.85	
UH ₈	Cubic	0	373.27	53.54	53.54	373.27	53.54	373.27	133.70	133.70	133.70	
	<i>Fm-3m</i>	30	603.30	104.23	104.23	603.30	104.23	603.30	184.16	184.16	184.16	
	225	40	682.30	127.99	127.99	682.30	127.99	682.30	198.92	198.92	198.92	
		50	731.74	143.45	143.45	731.74	143.45	731.74	213.15	213.15	213.15	[This]
		60	795.15	161.83	161.83	795.15	161.83	795.15	226.99	226.99	226.99	

Elastic/mechanical stability conditions of crystals with different structures under pressure are as follows [29-31].

For the orthorhombic structure:

$$C_{11} - P > 0, C_{22} - P > 0, C_{33} - P > 0, C_{44} - P > 0, C_{55} - P > 0, C_{66} - P > 0 \quad (2)$$

$$\text{and } (C_{11} + C_{22} - 2C_{12} - 4P) > 0, (C_{11} + C_{33} - 2C_{13} - 4P) > 0,$$

$$(C_{22} + C_{33} - 2C_{23} - 4P) > 0,$$

$$(C_{11} + C_{22} + C_{33} + 2C_{12} + 2C_{13} + 2C_{23} + 3P) > 0 \quad (3)$$

For the hexagonal structure:

$$\tilde{C}_{11} > 0; \tilde{C}_{33} > 0; \tilde{C}_{44} > 0; (\tilde{C}_{11} - \tilde{C}_{12}) > 0; (\tilde{C}_{11} + \tilde{C}_{12})\tilde{C}_{33} > 2\tilde{C}_{13}^2 \quad (4)$$

$$\text{where, } \tilde{C}_{\alpha\alpha} = C_{\alpha\alpha} - P, \alpha\alpha = 11, 33, 44, \tilde{C}_{12} = C_{12} + P, \tilde{C}_{13} = C_{13} + P$$

For the cubic structure:

$$M_1 = \frac{C_{11} + 2C_{12} + P}{3} > 0; M_2 = C_{44} - P > 0; M_3 = \frac{C_{11} - 2C_{12} - 2P}{2} > 0 \quad (5)$$

Our calculated results show that all the UH_x ($x = 1, 2, 3, 5, 6, 7, 8$) compounds with different structures satisfy the elastic stability conditions under pressure. Besides the calculated values of the tetragonal shear moduli are also positive (Table 3) which indicates that the structures are expected to be dynamically stable as well [32]. Results disclosed in Tables 2 and 3 are novel and no comparison with published sources can be made.

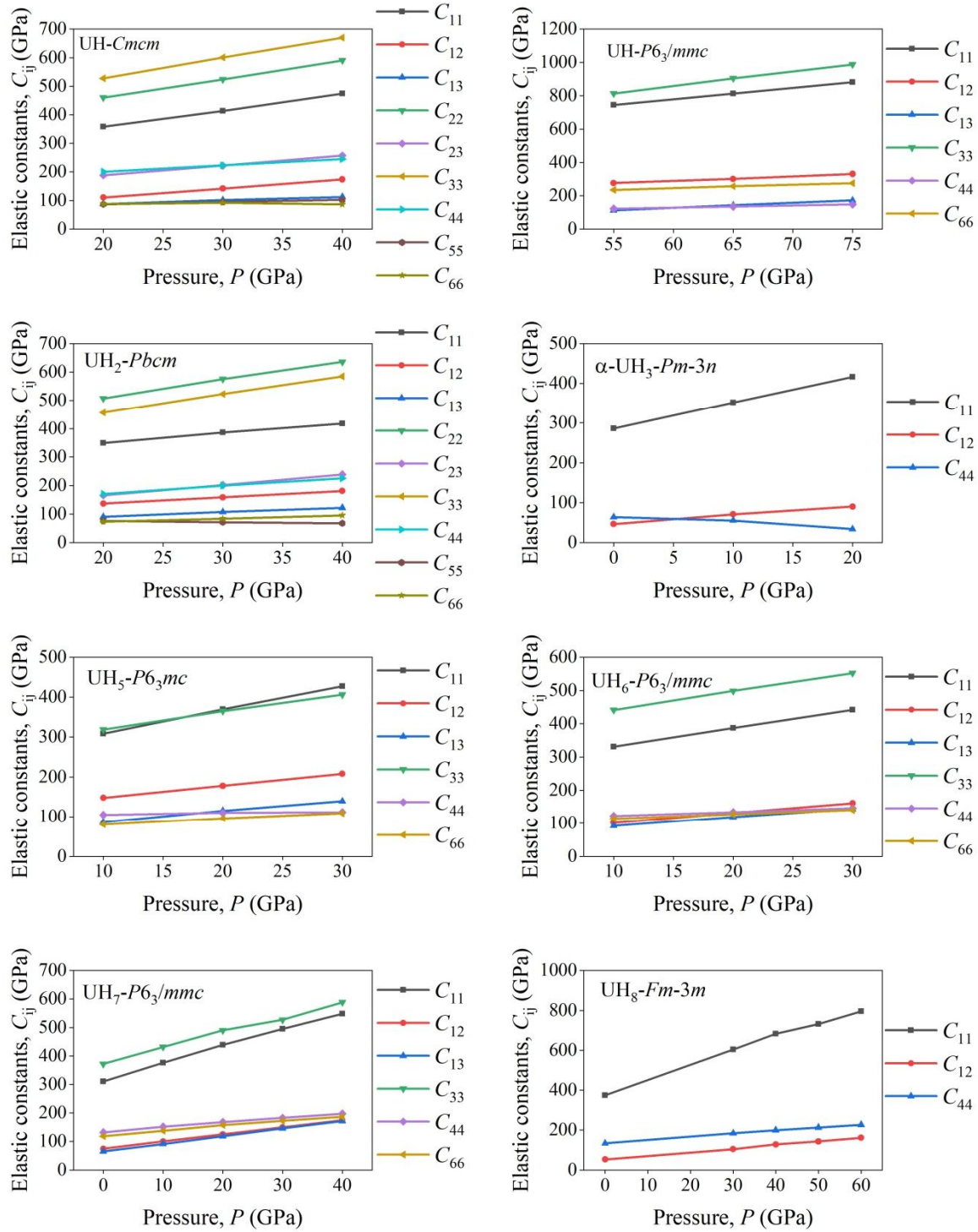


Figure 4: Elastic constants C_{ij} of UH_x ($x = 1, 2, 3, 5, 6, 7, 8$) compounds under different pressures.

Table 3. Calculated Cauchy pressure (GPa) and tetragonal shear modulus (TSM) (GPa) of UH_x ($x = 1, 2, 3, 5, 6, 7, 8$) compounds under different pressures.

Compounds	Crystal System Space Group Space Group No.	Pressure, P (GPa)	Cauchy Pressure (GPa)			TSM (GPa)	Ref.
			P_C^a	P_C^b	P_C^c		
			UH	Orthorhombic	20	-12.86	0.65
	<i>Cmcm</i>	30	-0.37	6.42	49.90	135.71	[This]
	63	40	12.47	9.94	87.44	150.12	
UH	Hexagonal	55	-11.01	42.57		233.78	
	$P6_3/mmc$	65	7.83	44.37		256.17	[This]
	194	75	24.64	55.00		275.09	
UH_2	Orthorhombic	20	-4.94	14.25	62.98	106.01	
	<i>Pbcm</i>	30	2.01	35.52	74.43	113.56	[This]
	57	40	13.97	54.21	85.09	117.98	
$\alpha\text{-UH}_3$	Cubic	0			-17.11	119.87	
	<i>Pm-3n</i>	10			15.64	140.24	[This]
	223	20			56.01	163.11	
UH_5	Hexagonal	10	-18.50	67.37		80.41	
	$P6_3mc$	20	5.19	82.10		95.88	[This]
	186	30	27.79	99.32		109.14	
UH_6	Hexagonal	10	-30.35	-13.57		114.87	
	$P6_3/mmc$	20	-15.20	3.69		127.79	[This]
	194	30	-2.48	20.61		140.41	
UH_7	Hexagonal	0	-67.20	-43.40		118.10	
	$P6_3/mmc$	10	-60.70	-37.08		137.44	
	194	20	-49.44	-31.77		156.84	[This]
		30	-36.62	-22.40		172.24	
		40	-25.41	-12.41		186.85	
UH_8	Cubic	0			-80.16	159.87	
	<i>Fm-3m</i>	30			-79.92	249.53	
	225	40			-70.92	277.15	
		50			-69.71	294.15	[This]
		60			-65.16	316.66	

The calculated values of Cauchy pressures (P_C) and tetragonal shear modulus are given in [Table 3](#). Cauchy pressure (P_C) is used to describe the brittleness and ductility of the compounds. Cauchy pressure (P_C) is defined for different crystal symmetries [32] as follows:

For orthorhombic symmetry: $P_C^a = (C_{23} - C_{44})$, $P_C^b = (C_{13} - C_{55})$ and $P_C^c = (C_{12} - C_{66})$

For hexagonal symmetry: $P_C^a = (C_{13} - C_{44})$ and $P_C^b = (C_{12} - C_{66})$

For cubic symmetry: $P_C^c = (C_{12} - C_{44})$

The values of P_C are negative for covalent materials with brittle nature (i.e. $P_C < 0$). Positive Cauchy pressure, on the other hand, suggests ductility with dominant ionic/metallic bonding where the outer shell electrons are almost delocalized [33]. The signs of at least one of the P_C are negative for UH-*Cmcm* at 20 and 30 GPa, for UH-*P6₃/mmc* at 55 GPa, for UH₂-*Pbcm* at 20 GPa, for α -UH₃-*Pm-3n* at 0 GPa, for UH₅-*P6₃mc* at 10 GPa, for UH₆-*P6₃/mmc* in the pressure range 10-30 GPa, for UH₇-*P6₃/mmc* in the pressure range 0-40 GPa, and for UH₈ in the pressure range 0-60 GPa. In some of the UH_{*x*} (*x* = 1, 2, 3, 5, 6, 7, 8) compounds, the negative Cauchy pressures take up positive values at elevated temperature and therefore, imply brittle-ductile transition. This could be related to increased level of metallicity in the UH_{*x*} materials with increasing pressure. The value of TSM used to measure the shear stiffness of a crystal i.e. the resistance to shear stress or shear deformation. TSM is also linked with the sound velocity in the solid. Positive values of TSM are indicative of dynamical stability of the structure. The polycrystalline elastic properties, namely the bulk modulus (*B*), shear modulus (*G*) and Young's modulus (*Y*) are given in Table 4. The values of Voigt [34], Reuss [35] and Hill [36] approximations are denoted by the subscripts *V*, *R* and *H*, respectively. Further details regarding the VRH approach can be found elsewhere [33-36]. Hill approximated elastic moduli are the average of the Voigt and Reuss approximated elastic moduli. From Table 4 (cf. Fig. 5) it is observed that elastic moduli increase systematically with pressure of all the UH_{*x*} compounds except the cubic α -UH₃-*Pm-3n*.

The bulk modulus represents the elastic resistance against uniform volume deformation. Large value of *B* signifies high incompressibility. Bulk modulus is also an average measure of the strength of interatomic bondings. From Table 4 it is observed that the bulk modulus increases with pressure for all the uranium hydrides under study. The shear modulus represents the elastic resistance against shape changing stress. High shear modulus is indicative of directional chemical bonding. From Table 4 it is found that the resistance to shape change increases with pressure of all the binary hydrides, except the cubic α -UH₃-*Pm-3n* compound. This exception is also found in case of the Young's modulus which represents the resistance against tensile stress. Young's modulus is a useful indicator of the stiffness of a solid. Thus it appears that, contrary to conventional behavior where elastic moduli increase with increasing pressure, the situation is reversed except in the cubic α -UH₃-*Pm-3n*. A possible reason might be that as pressure is

increased the bonding characters are modified and become less angular in nature. It is interesting to observe that, for UH, the hexagonal structure has significantly higher elastic moduli compared to the cubic one. This could be a consequence of greater packing fraction in the hexagonal structure.

Table 4. Polycrystalline elastic properties of UH_x ($x = 1, 2, 3, 5, 6, 7, 8$) compounds under different pressures.

Compounds	Crystal System Space Group Space Group No.	Pressure, P (GPa)	Polycrystalline elastic moduli (GPa)									Ref.
			Bulk, B (GPa)			Shear, G (GPa)			Young, Y (GPa)			
			B_V	B_R	B_H	G_V	G_R	G_H	Y_V	Y_R	Y_H	
UH	Orthorhombic	20	235.35	224.00	229.68	139.15	122.50	130.83	348.72	310.84	329.85	
	<i>Cmcm</i>	30	274.38	262.09	268.24	153.44	133.20	143.32	388.00	341.72	364.97	[This]
	63	40	313.45	300.46	306.96	166.10	138.90	152.50	423.50	361.07	392.51	
UH	Hexagonal	55	366.90	365.97	366.44	216.03	181.68	198.85	541.76	467.65	505.18	
	<i>P6₃/mmc</i>	65	411.41	411.00	411.20	234.84	198.51	216.67	591.90	512.94	552.91	[This]
	194	75	455.32	455.10	455.21	252.34	215.47	233.90	638.97	558.29	599.09	
UH ₂	Orthorhombic	20	232.95	222.46	227.70	125.31	108.71	117.01	318.78	280.44	299.69	
	<i>Pbcm</i>	30	268.72	254.53	261.63	138.84	116.26	127.55	355.33	302.71	329.17	[This]
	57	40	302.44	283.78	293.11	150.81	122.16	136.48	387.95	320.48	354.44	
α -UH ₃	Cubic	0	126.43	126.43	126.43	86.13	78.34	82.23	210.57	194.78	202.74	
	<i>Pm-3n</i>	10	164.57	164.57	164.57	89.36	73.12	81.24	226.99	191.06	209.28	[This]
	223	20	198.91	198.91	198.91	85.74	49.96	67.85	224.90	138.29	182.76	
UH ₅	Hexagonal	10	175.25	174.46	174.86	99.07	96.18	97.62	250.09	243.74	246.92	
	<i>P6₃mc</i>	20	213.41	212.16	212.79	109.55	107.66	108.61	280.63	276.25	278.44	[This]
	186	30	248.29	246.28	247.28	117.99	116.20	117.10	305.57	301.23	303.40	
UH ₆	Hexagonal	10	186.08	183.69	184.88	126.50	124.52	125.51	309.39	304.72	307.05	
	<i>P6₃/mmc</i>	20	223.59	221.48	222.53	139.49	137.49	138.49	346.43	341.75	344.09	[This]
	194	30	258.95	257.28	258.12	152.24	150.18	151.21	381.88	377.15	379.51	
UH ₇	Hexagonal	0	155.90	155.23	155.56	129.10	128.23	128.66	303.52	301.63	302.57	
	<i>P6₃/mmc</i>	10	194.14	193.64	193.89	148.18	147.50	147.84	354.37	352.90	353.64	
	194	20	232.26	231.86	232.06	165.48	165.05	165.27	401.17	400.19	400.68	[This]
		30	266.57	266.41	266.49	179.07	178.87	178.97	438.93	438.48	438.71	
		40	302.29	302.04	302.16	194.02	193.80	193.91	479.48	478.95	479.22	
UH ₈	Cubic	0	160.12	160.12	160.12	144.17	143.07	143.62	332.66	330.71	331.68	
	<i>Fm-3m</i>	30	270.59	270.59	270.59	210.31	205.71	208.01	501.10	492.37	496.74	
	225	40	312.76	312.76	312.76	230.21	224.24	227.22	554.57	542.95	548.78	
		50	339.54	339.54	339.54	245.55	239.54	242.54	593.57	581.79	587.69	[This]
		60	372.93	372.93	372.93	262.86	255.98	259.42	638.55	624.96	631.77	

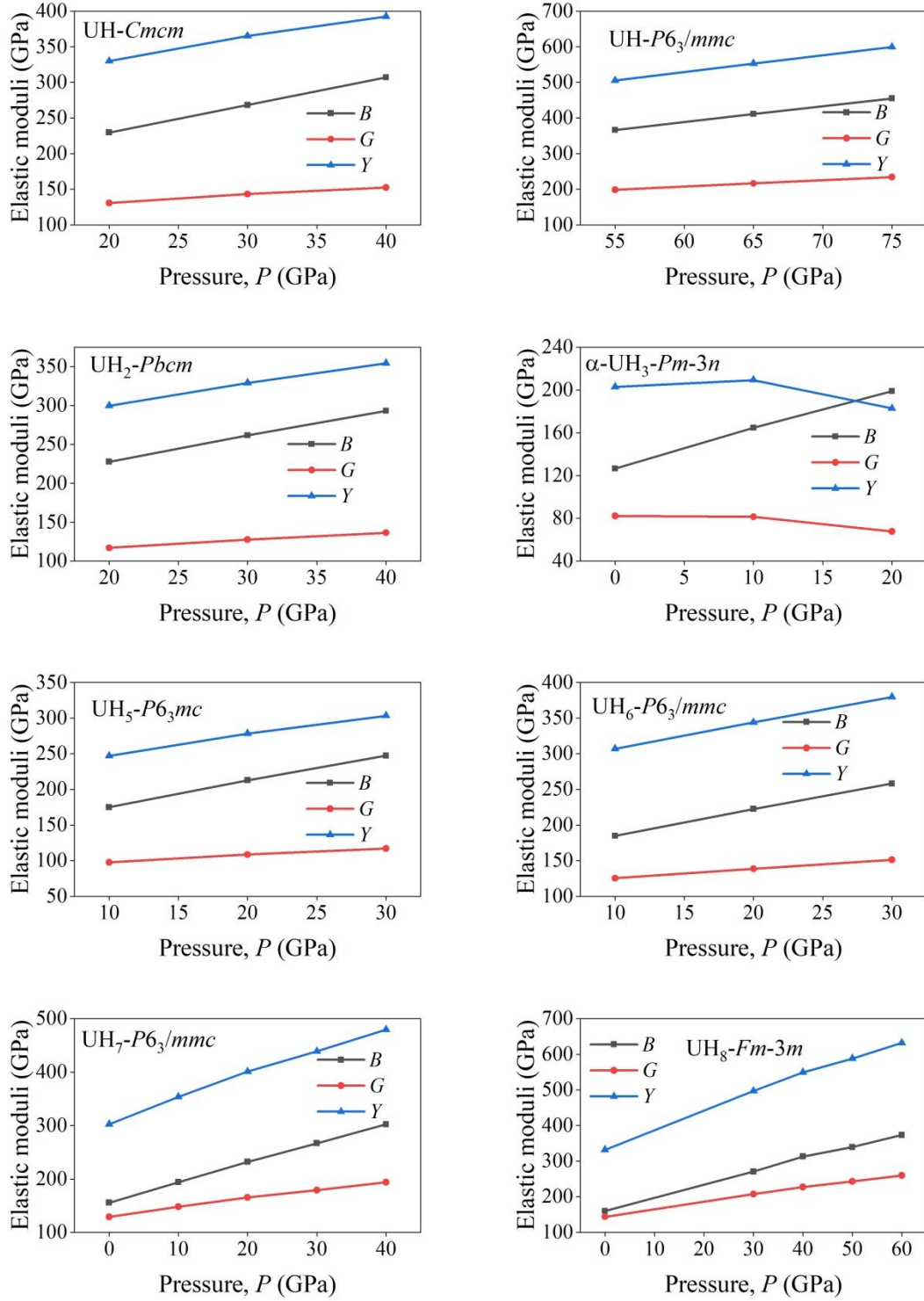


Figure 5: Elastic moduli of UH_x ($x = 1, 2, 3, 5, 6, 7, 8$) compounds under different pressures.

Table 5. Minimal and maximal values of the elastic moduli (Y and G), linear compressibility (β), and Poisson's ratio (ν) for UH_x ($x = 1, 2, 3, 5, 6, 7, 8$) compounds under different pressures.

Compounds	Crystal System Space Group Space Group No.	Pressure, P (GPa)	Young, Y (GPa)		Shear, G (GPa)		Linear compressibility (TPa ⁻¹)		Poisson's ratio		Ref.
			Y_{min}	Y_{max}	G_{min}	G_{max}	β_{min}	β_{max}	ν_{min}	ν_{max}	
UH	Orthorhombic	20	245.17	495.31	87.15	201.28	1.108	2.153	0.095	0.468	
	<i>Cmcm</i>	30	288.72	555.08	92.19	222.68	0.989	1.839	0.081	0.498	[This]
	63	40	268.00	615.96	86.19	244.99	0.830	1.591	0.087	0.560	
UH	Hexagonal	55	373.93	787.9	123.25	320.18	0.871	0.990	0.110	0.521	
	<i>P63/mmc</i>	65	410.97	868.4	134.88	345.95	0.788	0.856	0.114	0.528	[This]
	194	75	449.98	938.13	147.83	368.56	0.718	0.762	0.122	0.526	
UH ₂	Orthorhombic	20	219.7	428.66	73.351	170.51	0.932	2.134	0.108	0.536	
	<i>Pbcm</i>	30	215.49	497.65	71.695	199.7	0.778	1.933	0.111	0.542	[This]
	57	40	210.68	559.2	68.013	224.88	0.660	1.799	0.099	0.581	
α -UH ₃	Cubic	0	163.48	273.25	63.636	119.87	2.636	2.636	0.093	0.428	
	<i>Pm-3n</i>	10	149.51	327.66	55.432	140.24	2.026	2.026	0.089	0.561	[This]
	223	20	96.928	384.29	34.159	163.11	1.676	1.676	0.055	0.745	
UH ₅	Hexagonal	10	230.94	285.88	80.409	109.25	1.780	2.173	0.153	0.436	
	<i>P63mc</i>	20	269.32	316.43	95.878	122.72	1.441	1.832	0.181	0.425	[This]
	186	30	288.6	344.89	109.14	135.31	1.217	1.626	0.198	0.424	
UH ₆	Hexagonal	10	289.45	401.54	114.87	142.87	1.428	2.008	0.154	0.263	
	<i>P63/mmc</i>	20	326.38	443.94	127.79	158.05	1.218	1.649	0.170	0.287	[This]
	194	30	361.25	483.51	140.41	173.07	1.085	1.401	0.180	0.306	
		0	286.12	349.65	118.1	136.61	1.895	2.274	0.138	0.211	
UH ₇	Hexagonal	10	337.47	395.98	137.44	154.85	1.556	1.804	0.164	0.228	
	<i>P63/mmc</i>	20	387.44	439.54	156.84	172.08	1.320	1.497	0.185	0.235	[This]
	194	30	427.51	460.6	172.24	182.63	1.187	1.283	0.210	0.241	
UH ₈		40	466.94	506.3	186.85	197.78	1.036	1.138	0.219	0.249	
	Cubic	0	313.77	359.84	133.7	159.87	2.082	2.082	0.113	0.212	
	<i>Fm-3m</i>	30	450.31	572.59	184.16	249.53	1.232	1.232	0.122	0.292	
	225	40	492.37	641.86	198.92	277.15	1.066	1.066	0.129	0.314	
		50	528.8	684.72	213.15	294.15	0.982	0.982	0.134	0.315	[This]
		60	566.11	740.42	226.99	316.66	0.894	0.894	0.137	0.325	

Maximal and minimal values of various elastic moduli and Poisson's ratio are presented in [Table 5](#). These values were obtained from the ELATE [37] analysis of direction dependent elastic properties of UH_x ($x = 1, 2, 3, 5, 6, 7, 8$) compounds. The ratio between the maximum and minimum values is a measure of the direction dependent anisotropy in the atomic bonding within the crystals. From [Table 5](#) it is seen that anisotropy in the modulus of rigidity and Poisson's ratio is higher than the anisotropy in the Young's modulus and compressibility.

Table 6. Calculated Poisson's ratio (ν), Pugh's ratio (G/B), Grüneisen parameter (γ), and machinability index (μ_m) of UH_x ($x = 1, 2, 3, 5, 6, 7, 8$) compounds under different pressures.

Compounds	Crystal System Space Group Space Group No.	Pressure, P (GPa)	ν	G/B	γ	μ_m	Ref.
UH	Orthorhombic	20	0.26	0.57	1.55	1.14	
	<i>Cmcm</i>	30	0.27	0.53	1.62	1.20	[This]
	63	40	0.29	0.50	1.69	1.25	
UH	Hexagonal	55	0.27	0.54	1.60	2.97	
	<i>P63/mmc</i>	65	0.28	0.53	1.63	3.05	[This]
	194	75	0.28	0.51	1.66	3.08	
UH ₂	Orthorhombic	20	0.28	0.51	1.66	1.34	
	<i>Pbcm</i>	30	0.29	0.49	1.71	1.31	[This]
	57	40	0.30	0.47	1.76	1.30	
α -UH ₃	Cubic	0	0.23	0.65	1.42	1.99	
	<i>Pm-3n</i>	10	0.29	0.49	1.70	2.97	[This]
	223	20	0.35	0.34	2.11	5.82	
UH ₅	Hexagonal	10	0.26	0.56	1.57	1.67	
	<i>P63mc</i>	20	0.28	0.51	1.67	1.94	[This]
	186	30	0.30	0.47	1.75	2.21	
UH ₆	Hexagonal	10	0.22	0.68	1.38	1.51	
	<i>P63/mmc</i>	20	0.24	0.62	1.46	1.66	[This]
	194	30	0.25	0.59	1.52	1.77	
UH ₇	Hexagonal	0	0.18	0.83	1.20	1.18	
	<i>P63/mmc</i>	10	0.20	0.76	1.27	1.28	
	194	20	0.21	0.71	1.33	1.38	[This]
		30	0.23	0.67	1.39	1.46	
		40	0.24	0.64	1.43	1.53	
UH ₈	Cubic	0	0.15	0.90	1.13	1.20	
	<i>Fm-3m</i>	30	0.19	0.77	1.26	1.47	
	225	40	0.21	0.73	1.32	1.57	
		50	0.21	0.71	1.33	1.59	[This]
		60	0.22	0.70	1.36	1.64	

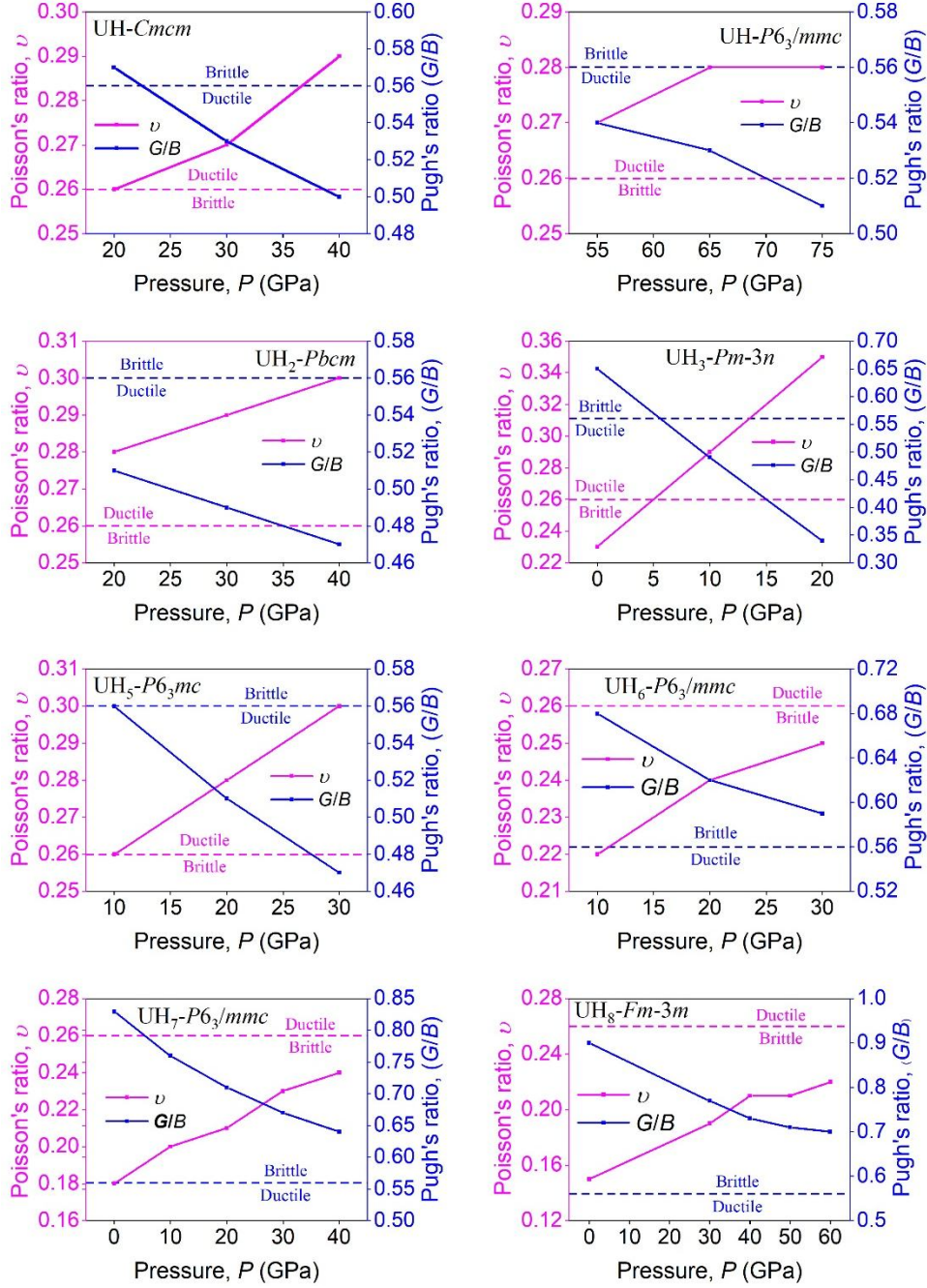


Figure 6: Poisson's and Pugh's ratio of UH_x ($x = 1, 2, 3, 5, 6, 7, 8$) compounds under different pressures.

The Poisson's ratio ν is calculated using the equation: $\nu = (3B - 2G)/(6B + 2G)$. The Pugh's ratio G/B and machinability index $\mu_m (= B/C_{44})$ are also computed and listed in Table 6. These three parameters are useful elastic/mechanical indicators. For example Poisson's ratio and Pugh's ratio can differentiate brittleness and ductility in solids. According to Frantsevich [38], if

$\nu > 0.26$ the solid should exhibit ductile nature otherwise it should be brittle. From [Table 6](#) and [Fig. 6](#) we see that the values of $\nu < 0.26$ for α -UH₃-Pm-3n at 0 GPa, for UH₆-P6₃/mmc in the pressure range 10-30 GPa, for UH₇-P6₃/mmc in the pressure range 0-40 GPa and from UH₈ in the pressure range 0-60 GPa the compounds are predicted to be brittle. On the other hand, $\nu > 0.26$ for UH-Cmcm at 30 and 40 GPa, for UH-P6₃/mmc within the pressure range 55-75 GPa, for UH₂-Pbcm within the pressure range 20-30 GPa, for α -UH₃-Pm-3n at 10 and 20 GPa, for UH₆-P6₃mc in the pressure range 10-30 GPa, ductility is expected. The Pugh's ratio (G/B) [39] is another parameter used to judge ductile and brittle nature of a solid [39]. $G/B > 0.57$ indicates the brittle nature and otherwise ductility. From [Table 6](#) and [Fig. 6](#) it is observed that the Pugh's ratio gives the same information about brittleness/ductility as the Poisson's ratio.

The machinability index determines the ease with which a solid can be shaped into desired form. It is also an indicator of dry lubricity of solids. High machinability index implies ease in the cutting and low level of frictional loss. For all the compounds under study, the machinability index increases systematically with increasing pressure. For the compound α -UH₃ in the cubic phase, μ_m is very high (5.82) at 20 GPa, suggesting that this compound becomes extremely machinable and should have excellent dry lubricity at high pressures.

Grüneisen parameter is related to the anharmonicity in the lattice dynamics. High value of Grüneisen parameter is indicative of strong electron-phonon interaction in superconductors [40]. This is because anharmonic and soft phonon modes contribute strongly to the electron-phonon coupling constant. The pressure dependent values of the Grüneisen parameter, calculated using the Poisson's ratio, are tabulated in [Table 6](#). The obtained values of γ are typical [41]. The highest value of the Grüneisen parameter (2.11) among all the compounds was found for α -UH₃ in the cubic phase at 20 GPa.

3.3 Elastic anisotropy

Study of the elastic anisotropy is important to understand the direction dependent bonding characteristics and mechanical properties of crystalline solids. The shear anisotropy factors [42] obtained from the elastic constants are given in [Table 7](#). These factors A_1 , A_2 , and A_3 are one for an isotropic crystal, while any value except unity is a measure of the degree of elastic anisotropy

possessed by the crystal. The factors A_1 , A_2 , and A_3 are computed from the expressions given below:

$$A_1 = \frac{4C_{44}}{C_{11} + C_{33} - 2C_{13}}, A_2 = \frac{4C_{55}}{C_{22} + C_{33} - 2C_{23}}, A_3 = \frac{4C_{66}}{C_{11} + C_{22} - 2C_{12}} \quad (6)$$

Furthermore, A^B and A^G are the percentage anisotropies in compressibility and shear, respectively, and A^U is the universal anisotropy index. The zero values of A^B , A^G and A^U represent elastic isotropy of a crystal and non-zero values represent anisotropy [43, 44]. The computed values of A^U , A^B , and A^G are also listed in Table 7. These anisotropy indices are calculated using the following equations:

$$A^B = \frac{B_V - B_R}{B_V + B_R}, A^G = \frac{G_V - G_R}{G_V + G_R}, \text{ and } A^U = 5 \frac{G_V}{G_R} + \frac{B_V}{B_R} - 6 \geq 0 \quad (7)$$

Table 7 (and Fig. 7) shows clearly that the UH_x ($x = 1, 2, 3, 5, 6, 7, 8$) compounds are elastically anisotropic. These anisotropies are clear indications that atomic bonding strengths in different directions in the crystals are different. Among the compounds of interest, hexagonal UH_7 - $P6_3/mmc$ has the lowest anisotropy because $A_1 = A_2 = A_3 = 1$ and A^U , A^B and A^G values are very close to zero in the pressure range 30 – 40 GPa. Overall the orthorhombic UH - $Cmcm$ has the highest level of anisotropy. The pressure dependent variations in various anisotropy indices are nonmonotonic, indicating that changes in the bonding characters are different in different crystal directions when uniform hydrostatic pressure is applied. Fig. 7 shows these variations clearly.

Table 7. The shear anisotropy factors A_1 , A_2 , A_3 , and A^B (in %), A^G (in %), A^U of UH_x ($x = 1, 2, 3, 5, 6, 7, 8$) compounds under different pressures.

Compounds	Crystal System Space Group Space Group No.	Pressure, P (GPa)	A_1	A_2	A_3	A^B	A^G	A^U	Ref.
UH	Orthorhombic	20	1.13	0.57	0.59	2.47	6.36	0.73	
	$Cmcm$	30	1.10	0.56	0.56	2.29	7.06	0.81	[This]
	63	40	1.07	0.55	0.48	2.11	8.92	1.02	
UH	Hexagonal	55	0.37	0.37	1.00	0.13	8.64	0.95	
	$P6_3/mmc$	65	0.38	0.38	1.00	0.05	8.38	0.92	[This]
	194	75	0.39	0.39	1.00	0.03	7.88	0.86	
UH_2	Orthorhombic	20	1.09	0.48	0.50	2.30	7.10	0.81	
	$Pbcm$	30	1.15	0.41	0.52	2.71	8.85	1.03	[This]

	57	40	1.19	0.37	0.56	3.18	10.50	1.24	
α -UH ₃	Cubic	0	0.53	0.53	0.53	0.00	4.74	0.50	
	<i>Pm-3n</i>	10	0.40	0.40	0.40	0.00	9.99	1.11	
	223	20	0.21	0.21	0.21	0.00	26.37	3.58	
UH ₅	Hexagonal	10	0.92	0.92	1.00	0.22	1.48	0.16	
	<i>P6₃mc</i>	20	0.87	0.87	1.00	0.29	0.87	0.09	[This]
	186	30	0.81	0.81	1.00	0.40	0.76	0.09	
UH ₆	Hexagonal	10	0.83	0.83	1.00	0.65	0.79	0.09	
	<i>P6₃/mmc</i>	20	0.83	0.83	1.00	0.47	0.72	0.08	[This]
	194	30	0.82	0.82	1.00	0.32	0.68	0.08	
UH ₇	Hexagonal	0	0.96	0.96	1.00	0.21	0.34	0.04	
	<i>P6₃/mmc</i>	10	0.97	0.97	1.00	0.13	0.23	0.03	
	194	20	0.97	0.97	1.00	0.09	0.13	0.01	[This]
		30	1.00	1.00	1.00	0.03	0.06	0.01	
		40	1.00	1.00	1.00	0.04	0.06	0.01	
UH ₈	Cubic	0	0.84	0.84	0.84	0.00	0.38	0.04	
	<i>Fm-3m</i>	10	0.74	0.74	0.74	0.00	1.10	0.11	
	225	40	0.72	0.72	0.72	0.00	1.31	0.13	
		50	0.72	0.72	0.72	0.00	1.24	0.13	[This]
		60	0.72	0.72	0.72	0.00	1.32	0.13	

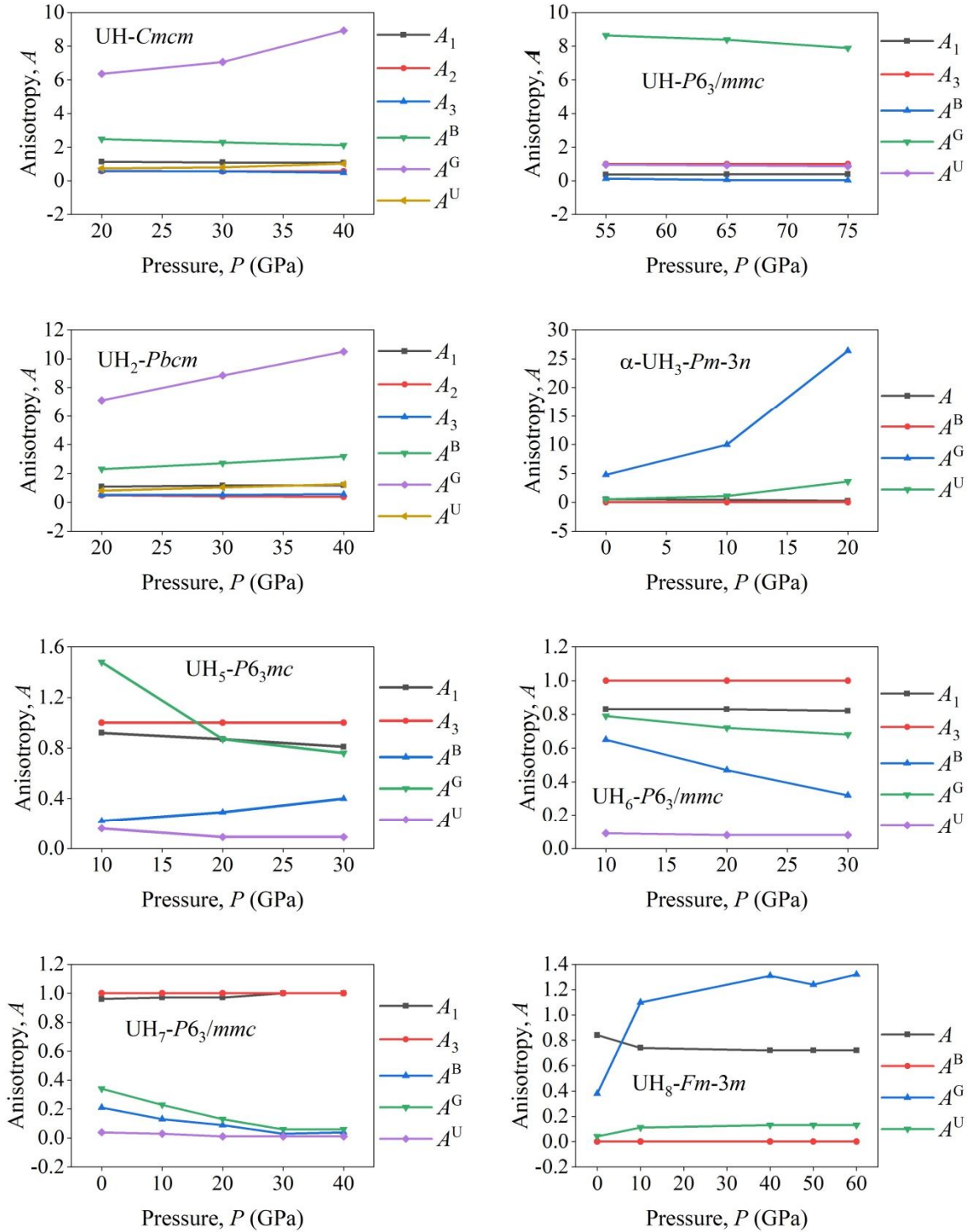


Figure 7: Anisotropy indices of UH_x ($x = 1, 2, 3, 5, 6, 7, 8$) compounds under different pressures.

3.4 Acoustic velocities

The sound velocities in a crystal are useful thermophysical parameter. These velocities are closely related to the crystal stiffness and crystal density, and determine the Debye temperature and thermal conductivity to a large extent [45]. Crystalline solids support both longitudinal and transverse modes of propagation of acoustic disturbances. The phonon thermal conductivity of solids increases with increasing acoustic velocities.

Table 8. Calculated density ρ (gm/cm³), transverse sound velocities v_t (km/s), longitudinal sound velocities v_l (km/s), average sound velocities v_m (km/s), Debye temperature θ_D (K) and melting temperature T_m (K) of UH_x ($x = 1, 2, 3, 5, 6, 7, 8$) compounds under different pressures.

Compounds	Crystal System Space Group Space Group No.	Pressure, P (GPa)	ρ	v_t	v_l	v_m	θ_D	T_m	Ref
UH	Orthorhombic	20	18.68	2.6464	4.6512	2.9417	398.41	2218.34	
	<i>Cmcm</i>	30	19.46	2.7138	4.8583	3.0212	414.80	2495.30	[This]
	63	40	20.17	2.7499	5.0303	3.0666	426.06	2780.27	
UH	Hexagonal	55	21.98	3.0080	5.3607	3.3475	478.61	3804.63	
	<i>P6₃/mmc</i>	65	22.55	3.0996	5.5716	3.4518	497.80	4150.13	[This]
	194	75	23.08	3.1835	5.7652	3.5474	515.52	4475.74	
UH ₂	Orthorhombic	20	16.13	2.6934	4.8774	3.0011	442.45	2083.43	
	<i>Pbcm</i>	30	16.82	2.7535	5.0656	3.0719	459.27	2294.97	[This]
	57	40	17.46	2.7959	5.2165	3.1224	472.63	2482.08	
α -UH ₃	Cubic	0	12.06	2.6108	4.4237	2.8928	425.47	1642.15	
	<i>Pm-3n</i>	10	12.92	2.5073	4.5953	2.7964	420.84	1936.02	[This]
	223	20	13.65	2.2292	4.6037	2.5052	384.00	2227.75	
UH ₅	Hexagonal	10	11.20	2.9520	5.2180	3.2830	537.78	1757.75	
	<i>P6₃mc</i>	20	11.79	3.0351	5.5074	3.3825	563.59	2010.43	[This]
	186	30	12.31	3.0839	5.7241	3.4427	581.98	2243.46	
UH ₆	Hexagonal	10	10.63	3.4369	5.7576	3.8040	643.61	2008.54	
	<i>P6₃/mmc</i>	20	11.17	3.5217	6.0386	3.9062	671.95	2263.19	[This]
	194	30	11.64	3.6043	6.2847	4.0038	698.32	2506.96	
		0	9.86	3.6115	5.7585	3.9769	685.36	1844.10	
UH ₇	Hexagonal	10	10.44	3.7624	6.1187	4.1518	729.24	2126.23	
	<i>P6₃/mmc</i>	20	10.94	3.8868	6.4309	4.2967	766.43	2404.09	
	194	30	11.38	3.9649	6.6609	4.3895	793.47	2627.19	
		40	11.79	4.0550	6.8955	4.4944	822.02	2880.52	
UH ₈		0	9.65	3.8585	6.0374	4.2399	753.26	2033.72	
	Cubic	10	11.11	4.3276	7.0237	4.7745	889.05	3068.84	

	<i>Fm-3m</i>	40	11.49	4.4468	7.3200	4.9132	925.30	3424.33	[This]
	225	50	11.85	4.5236	7.4786	5.0002	951.47	3646.83	
		60	12.19	4.6131	7.6789	5.1026	980.08	3932.16	

The calculated values of sound velocities (v_t , v_l and v_m) under pressure of UH_x compounds are listed in Table 8. The following equations were used to determine the sound velocities [46-48]:

$$v_t = \sqrt{\frac{G}{\rho}}, v_l = \sqrt{\frac{3B + 4G}{3\rho}} \text{ and } v_m = \left[\frac{1}{3} \left(\frac{2}{v_t^3} + \frac{1}{v_l^3} \right) \right]^{-\frac{1}{3}} \quad (8)$$

In the above equations v_t , v_l and v_m signify the transverse, longitudinal, and the mean sound velocities, respectively. The computed values of sound velocities at different pressures are enlisted in Table 8. The pressure dependent variations in the sound velocities are also illustrated in Fig. 8 for all the compounds under study. In general, the sound velocities increase with increasing pressure due to the increase in the crystal stiffness. This is seen in all the UH_x compounds, except the cubic α - UH_3 - $Pm-3n$ compound. This particular compound also shows unconventional variation of the elastic moduli with pressure variation.

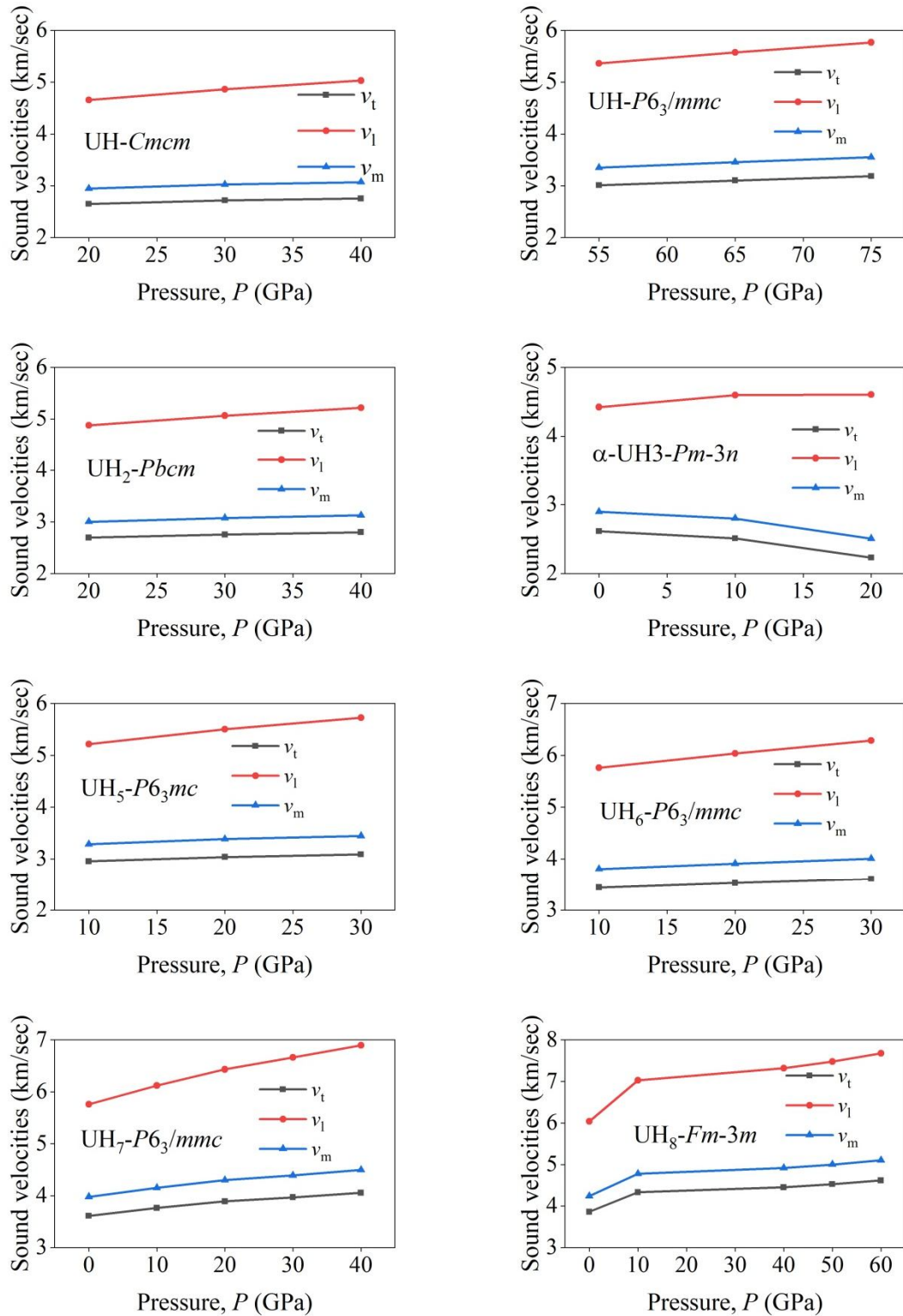


Figure 8: Sound velocities in UH_x ($x = 1, 2, 3, 5, 6, 7, 8$) compounds under different pressures.

3.5 Hardness of UH_x compounds

Hardness of a solid is used to assess both elastic and plastic behaviors of the material under mechanical stress. This particular parameter determines the average bonding strength and stiffness of a solid. A variety of theoretical methodologies are available to compute the hardness of a solid. In this study, we have calculated the hardness of the UH_x ($x = 1, 2, 3, 5, 6, 7, 8$) compounds at different pressures using the formalisms developed by Teter et al. [49], Tian et al. [50], Chen et al. [51], microhardness [52], and Efim Mazhnik [53]. The calculated values of hardness are presented in Table 9. The pressure dependent hardness values are also illustrated in Fig. 9 showing that different formalisms result in different values of hardness. Considering the highest values of the hardness, the calculated values according to Teter et al. are arranged in the following order: $UH-P6_3/mmc > UH_8-Fm-3m > UH-Cmcm > UH_7-P6_3/mmc > UH_6-P6_3/mmc > UH_2-Pbcm > UH_5-P6_3mc > \alpha-UH_3-Pm-3n$. According to Tian et al., the hardnesses are arranged in the following order: $UH_8-Fm-3m > UH_7-P6_3/mmc > UH-P6_3/mmc > UH_6-P6_3/mmc > UH-Cmcm > \alpha-UH_3-Pm-3n > UH_2-Pbcm > UH_5-P6_3mc$. According to Chen et al., the hardnesses are arranged in the following order: $UH_8-Fm-3m > UH_7-P6_3/mmc > UH-P6_3/mmc > UH_6-P6_3/mmc > UH-Cmcm > \alpha-UH_3-Pm-3n > UH_5-P6_3mc > UH_2-Pbcm$. According to microhardness, the hardnesses values arranged in the following order: $UH_8-Fm-3m > UH-P6_3/mmc > UH_7-P6_3/mmc > UH_6-P6_3/mmc > UH-Cmcm > UH_2-Pbcm > UH_5-P6_3mc > \alpha-UH_3-Pm-3n$. According to Efim-Mazhnik, the hardnesses values are arranged in the following order: $UH_8-Fm-3m > UH-P6_3/mmc > UH_7-P6_3/mmc > UH-Cmcm > UH_2-Pbcm > UH_6-P6_3/mmc > UH_5-P6_3mc > \alpha-UH_3-Pm-3n$. It is interesting to note that the microhardness value of the cubic $UH_8-Fm-3m$ is extremely high at high pressures and this compound can be classified as a superhard solid. Overall, among all the binary uranium hydrides considered, the cubic $\alpha-UH_3-Pm-3n$ phase seems to be the least hard. It should be stressed here that comparison among the hardness values in this section is rough measures since the pressures are different for the different structures. Nevertheless, the comparisons have been made with extrapolations and therefore, should result in fairly reliable conclusions.

Table 9. Hardness of UH_x ($x = 1, 2, 3, 5, 6, 7, 8$) compounds under different pressures.

Compounds	Crystal System Space Group Space Group No.	Pressure, P (GPa)	Hardness H (GPa)					Ref.
			H_{Teter}	H_{Tian}	H_{Chen}	H_{micro}	$H_{\text{Efim Mazhnik}}$	
UH	Orthorhombic	20	19.75	13.41	14.92	20.88	15.78	
	<i>Cmcm</i>	30	21.64	13.11	14.54	21.67	18.01	[This]
	63	40	23.03	12.40	13.70	21.67	20.04	
UH	Hexagonal	55	30.03	16.88	18.63	30.46	24.74	
	<i>P6₃/mmc</i>	65	32.72	17.23	18.97	32.37	27.47	[This]
	194	75	35.32	17.57	19.31	34.20	30.12	
UH ₂	Orthorhombic	20	17.67	10.76	11.88	17.11	15.07	
	<i>Pbcm</i>	30	19.26	10.65	11.72	17.83	16.94	[This]
	57	40	20.61	10.49	11.51	18.34	18.57	
α -UH ₃	Cubic	0	12.42	11.58	12.95	14.65	9.42	
	<i>Pm-3n</i>	10	12.27	7.87	8.47	11.48	10.71	[This]
	223	20	10.25	4.17	3.70	6.93	10.26	
UH ₅	Hexagonal	10	14.74	10.61	11.75	15.32	11.93	
	<i>P6₃mc</i>	20	16.40	10.12	11.13	15.79	14.04	
	186	30	17.68	9.63	10.53	15.96	15.79	
UH ₆	Hexagonal	10	18.95	16.57	18.48	23.16	14.53	
	<i>P6₃/mmc</i>	20	20.91	15.77	17.55	23.79	15.97	[This]
	194	30	22.83	15.44	17.15	24.70	17.93	
UH ₇	Hexagonal	0	19.43	22.10	24.45	27.81	19.13	
	<i>P6₃/mmc</i>	10	22.32	21.81	24.08	29.96	19.39	
	194	20	24.96	21.49	23.68	31.71	19.84	
		30	27.02	20.98	23.10	32.74	20.63	
		40	29.28	20.87	22.93	34.17	22.22	
UH ₈	Cubic	0	21.69	26.69	29.19	33.06	23.69	
	<i>Fm-3m</i>	10	31.41	28.09	30.38	42.43	27.62	
	225	40	34.31	27.67	29.90	44.30	27.88	
		50	36.62	28.32	30.51	46.64	29.20	[This]
		60	39.17	28.64	30.79	48.83	30.50	

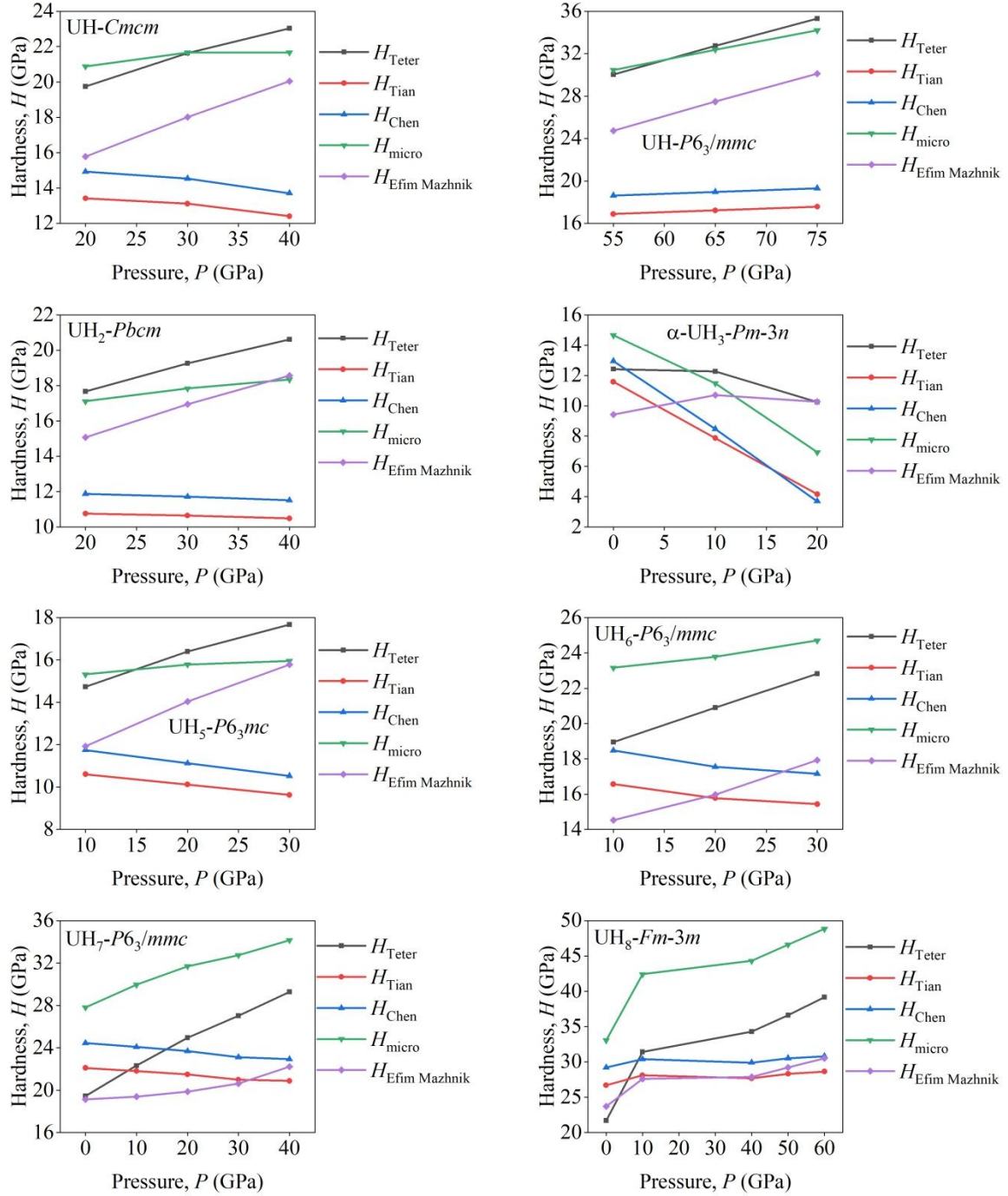


Figure 9: Hardness of UH_x ($x = 1, 2, 3, 5, 6, 7, 8$) compounds under different pressures.

3.6 Thermophysical properties of UH_x compounds

Debye temperature: The Debye temperature θ_D of a system is closely connected to many major physical properties of solids such as the phonon specific heat, melting temperature, thermal conductivity, hardness, elastic constants, bonding strength, and sound velocity. The knowledge of θ_D provides information about the electron-phonon coupling and Cooper pairing mechanism of superconductivity. The Debye temperature calculated from the elastic constants is considered to be similar to that acquired from the temperature dependent specific heat measurements. Using the average sound velocity, the Debye temperature can be calculated by using the Anderson method [54] as follows:

$$\theta_D = \frac{h}{k_B} \left[\left(\frac{3n}{4\pi} \right) \frac{N_A \rho}{M} \right]^{1/3} v_m \quad (9)$$

where, h is Planck's constant, k_B is the Boltzmann's constant, ρ is the density, N_A is the Avogadro number, M is the molecular mass, and v_m is the average sound velocity. This particular straightforward approach gives very reliable values of the Debye temperature of solids belonging to diverse categories (insulators, metals, topological compounds, magnetic materials, and superconductors) [55-59]. The computed results of the binary uranium hydrides are disclosed in Table 8. UH_8 in the cubic phase has the highest Debye temperature. The hardness of this compound is also the highest. It is worth noticing that, among all the hydrides under investigation, the predicted superconducting transition temperature of this particular one is the highest. We believe that high predicted T_c in this compound is partly due to its very high Debye temperature. In conventional phonon mediated superconductors, the superconducting transition temperature is directly proportional to the Debye temperature. The pressure induced increase in the Debye temperature suggests that for superconducting compositions, the T_c should increase with increasing pressure provided that the electron-phonon coupling constant does not decrease significantly due to the increase in the pressure.

Minimum thermal conductivity: At temperatures above θ_D the thermal conductivity of a solid attains a minimum value known as the minimum thermal conductivity, κ_{min} . The calculated values of the minimum thermal conductivity are derived from the relation given by $\kappa_{min} =$

$k_B v_m (V_a)^{-2/3}$ [60] and presented in Table 10. The minimum thermal conductivity is determined by the scattering dynamics of the phonons in a solid.

Grüneisen parameter: The Grüneisen parameter γ is an important thermophysical quantity that links the vibrational properties with the structural ones. It is related to the thermal expansion coefficient, bulk modulus, specific heat, and electron-phonon coupling in solids. The normal thermal expansion of solids due to anharmonicity of interatomic forces is understood from the Grüneisen constant as well. The relation between Grüneisen parameter and Poisson's ratio is as follows: $\gamma = \frac{3}{2} \frac{1+\nu}{2-3\nu}$ [61]. The calculated values of Grüneisen parameters at different pressures are presented in Table 6.

Melting temperature: Information on the melting temperature of a compound is very important for practical applications of solids at high temperatures. High melting temperature of a compound has lower thermal expansion and high binding energy. We have calculated the melting temperature T_m of UH_x ($x = 1, 2, 3, 5, 6, 7, 8$) compounds at different pressures using the following equation [62]:

$$T_m = 354 + \frac{4.5(2C_{11} + C_{33})}{3} \quad (10)$$

The calculated values of melting temperatures are listed in Table 8. The melting temperatures of are very high at different pressures for all the UH_x compounds under study. In particular, the melting temperature of UH in the hexagonal phase approaches 4475 K at a pressure of 75 GPa. The high values of melting temperatures predict excellent thermal study of the UH_x ($x = 1, 2, 3, 5, 6, 7, 8$) compounds. These high values show good correlation with the previously estimated bulk moduli, Debye temperatures, and hardnesses. The melting temperature increases systematically with the increase in the pressure for all the UH_x structures considered in our calculations.

Table 10. Thermal expansion coefficient α (10^{-5} K^{-1}) and minimum thermal conductivity, k_{\min} ($\text{Wm}^{-1}\text{K}^{-1}$) of UH_x ($x = 1, 2, 3, 5, 6, 7, 8$) compounds under different pressures.

Compounds	Crystal System Space Group Space Group No.	Pressure P (GPa)	α	k_{\min}		Ref.
				Cahill	Clark	
UH	Orthorhombic	20	1.22	1.15	0.84	
	<i>Cmcm</i>	30	1.12	1.22	0.89	[This]
	63	40	1.05	1.28	0.92	
UH	Hexagonal	55	0.80	1.46	1.07	
	<i>P6₃/mmc</i>	65	0.74	1.54	1.12	[This]
	194	75	0.68	1.61	1.17	
UH ₂	Orthorhombic	20	1.37	1.40	1.02	
	<i>Pbcm</i>	30	1.25	1.48	1.07	[This]
	57	40	1.17	1.56	1.11	
α -UH ₃	Cubic	0	1.95	1.31	0.97	
	<i>Pm-3n</i>	10	1.97	1.37	0.99	[This]
	223	20	2.36	1.34	0.92	
UH ₅	Hexagonal	10	1.64	1.87	1.37	
	<i>P6₃mc</i>	20	1.47	2.02	1.46	[This]
	186	30	1.37	2.13	1.53	
UH ₆	Hexagonal	10	1.27	2.27	1.70	
	<i>P6₃/mmc</i>	20	1.16	2.43	1.80	[This]
	194	30	1.06	2.58	1.90	
UH ₇	Hexagonal	0	1.24	2.42	1.84	
	<i>P6₃/mmc</i>	10	1.08	2.64	1.99	
	194	20	0.97	2.84	2.13	[This]
		30	0.89	2.99	2.23	
UH ₈		40	0.83	3.15	2.34	
	Cubic	0	1.11	2.73	2.08	
	<i>Fm-3m</i>	10	0.77	3.41	2.58	
	225	40	0.70	3.61	2.71	
		50	0.66	3.76	2.82	[This]
		60	0.62	3.92	2.93	

Thermal expansion coefficient: The thermal expansion coefficient (TEC) of a material is connected to many other thermal and electronic properties, such as thermal conductivity, heat capacity, temperature variation of the energy band gap of semiconductors and temperature

variation of the electron/hole effective mass. The thermal expansion coefficient of a material can be estimated using the following equation [63]:

$$\alpha = \frac{1.6 \times 10^{-3}}{G} \quad (11)$$

The relation between thermal expansion coefficient and the melting temperature can be also approximated as $\alpha \approx 0.02/T_m$. The values of thermal expansion coefficient of UH_x ($x = 1, 2, 3, 5, 6, 7, 8$) compounds under different pressures are also given in Table 10. The calculated values of the TEC follow roughly inverse trend with the melting temperature as expected. The lowest TEC is found for the cubic UH_8 compound. This compound also has the largest minimal thermal conductivity. The highest TEC is obtained for the cubic $\alpha\text{-UH}_3\text{-Pm-3n}$ phase; a result consistent with the other thermo-mechanical parameters.

4. Conclusions

In this work we have studied the structural, elastic, mechanical and thermophysical properties of a series of already synthesized and predicted binary uranium hydrides with different structures under hydrostatic pressure. Most of the results presented are novel. These compounds have the potential to show high superconducting critical temperature as well as applications in hydrogen storage systems. The UH_x ($x = 1, 2, 3, 5, 6, 7, 8$) compounds are found to be elastically stable and anisotropic with varying degree. All the compounds are fairly hard with the cubic UH_8 compound showing superhard behavior at high pressure. The compounds are highly machinable and the cubic $\alpha\text{-UH}_3\text{-Pm-3n}$ compound possesses extremely high machinability and dry lubricity at 20 GPa. Most of the compounds are brittle in nature at lower pressures while there is clear indication of brittle-to-ductile transformation at high pressures. The Debye temperatures and sound velocities are high. The highest Debye temperature was obtained for the cubic UH_8 compound for which a very high superconducting transition temperature has been predicted at elevated pressure. We have also calculated the cohesive energy for all the binary compounds. The positive values of cohesive energy indicate chemical stability of UH_x . The values of enthalpies increase with pressure indicating phase stability, except for $\text{UH}_8\text{-Fm-3m}$. All the compounds under study show medium lattice anharmonicity. The melting temperatures are high, consistent with the elastic properties and Debye temperatures. The thermal expansion coefficient

and minimal phonon thermal conductivity of the UH_x ($x = 1, 2, 3, 5, 6, 7, 8$) compounds also corresponds well with the other thermo-mechanical characteristics.

Acknowledgements

S. H. N. acknowledges the research grant (1151/5/52/RU/Science-07/19-20) from the Faculty of Science, University of Rajshahi, Bangladesh, which partly supported this work. Md. A. A. acknowledges the financial support from the Bangabandhu Science and Technology Fellowship Trust for his Ph.D. research.

Data availability

The data sets generated and/or analyzed in this study are available from the corresponding author on reasonable request.

Declaration of interest

The authors declare that they have no known competing financial interests or personal relationships that could have appeared to influence the work reported in this paper.

References

- [1] Ashcroft, N. W. (1968). Metallic hydrogen: A high-temperature superconductor? *Physical Review Letters*, *21*(26), 1748.
- [2] Sieverts, A., & Bergner, E. (1912). Versuche über die Löslichkeit von Argon und Helium in festen und flüssigen Metallen. *Berichte der deutschen chemischen Gesellschaft*, *45*(2), 2576-2583.
- [3] Driggs F. H., *United States Patent* (1931), 1835024.
- [4] Mulford, R. N. R., Ellinger, F. H., & Zachariasen, W. H. (1954). A new form of uranium hydride1. *Journal of the American Chemical Society*, *76*(1), 297-298.
- [5] Liu, M., Shi, Y., Liu, M., Li, D., Mo, W., Fa, T., & Chen, X. (2020). First-principles comprehensive study of electronic and mechanical properties of novel uranium hydrides at different pressures. *Progress in Natural Science: Materials International*, *30*(2), 251-259.
- [6] Eremets, M. I., Trojan, I. A., Medvedev, S. A., Tse, J. S., & Yao, Y. (2008). Superconductivity in Hydrogen Dominant Materials: Silane. *Science*, *319*(5869), 1506–1509.
- [7] Drozdov, A. P., Eremets, M. I., Troyan, I. A., Ksenofontov, V., & Shylin, S. I. (2015). Conventional superconductivity at 203 kelvin at high pressures in the sulfur hydride system. *Nature*, *525*(7567), 73-76.
- [8] Troyan, I., Drozdov, A. P., Eremets, M. I., Gavriliuk, A., Lyubutin, I., Mironovich, A., & Perekalin, D. (2016). Observation of superconductivity in hydrogen sulfide from nuclear resonant scattering. *Science*, *351*(6279), 1303-1306.

- [9] Gao, G., Wang, L., Li, M., Zhang, J., Howie, R. T., Gregoryanz, E., & John, S. T. (2021). Superconducting binary hydrides: Theoretical predictions and experimental progresses. *Materials Today Physics*, *21*, 100546.
- [10] Duan, D., Liu, Y., Tian, F., Li, D., Huang, X., Zhao, Z., & Cui, T. (2014). Pressure-induced metallization of dense $(\text{H}_2\text{S})_2\text{H}_2$ with high- T_c superconductivity. *Scientific reports*, *4*(1), 6968.
- [11] Chung, D., Lee, J., Koo, D., Chung, H., Kim, K. H., Kang, H. G., & Lee, H. (2013). Hydriding and dehydriding characteristics of small-scale DU and ZrCo beds. *Fusion Engineering and Design*, *88*(9-10), 2276-2279.
- [12] Banos, A., Harker, N. J., & Scott, T. B. (2018). A review of uranium corrosion by hydrogen and the formation of uranium hydride. *Corrosion Science*, *136*, 129-147.
- [13] Yoo, H., Kim, W., & Ju, H. (2014). A numerical comparison of hydrogen absorption behaviors of uranium and zirconium cobalt-based metal hydride beds. *Solid State Ionics*, *262*, 241-247.
- [14] Manchester, F. D., & San-Martin, A. (1995). The HU (hydrogen-uranium) system. *Journal of phase equilibria*, *16*(3), 263-275.
- [15] Bloch, J. (2003). The hydriding kinetics of activated uranium powder under low (near equilibrium) hydrogen pressure. *Journal of alloys and compounds*, *361*(1-2), 130-137.
- [16] Kruglov, I. A., Kvashnin, A. G., Goncharov, A. F., Oganov, A. R., Lobanov, S. S., Holtgrewe, N., & Yanilkin, A. V. (2018). Uranium polyhydrides at moderate pressures: Prediction, synthesis, and expected superconductivity. *Science advances*, *4*(10), eaat9776.
- [17] Wang, X., Li, M., Zheng, F., & Zhang, P. (2018). Crystal structure prediction of uranium hydrides at high pressure: A new hydrogen-rich phase. *Physics Letters A*, *382*(40), 2959-2964.
- [18] Souter, P. F., Kushto, G. P., Andrews, L., & Neurock, M. (1997). Experimental and Theoretical Evidence for the Formation of Several Uranium Hydride Molecules. *Journal of the American Chemical Society*, *119*(7), 1682-1687.
- [19] Raab, J., Lindh, R. H., Wang, X., Andrews, L., & Gagliardi, L. (2007). A Combined Experimental and Theoretical Study of Uranium Polyhydrides with New Evidence for the Large Complex $\text{UH}_4(\text{H}_2)_6$. *The Journal of Physical Chemistry A*, *111*(28), 6383-6387.
- [20] Kohn, W., & Sham, L. J. (1965). Self-consistent equations including exchange and correlation effects. *Physical Review*, *140*(4A), A1133.
- [21] Clark, S. J., Segall, M. D., Pickard, C. J., Hasnip, P. J., Probert, M. I., Refson, K., & Payne, M. C. (2005). First principles methods using CASTEP. *Zeitschrift für Kristallographie-Crystalline Materials*, *220*(5-6), 567-570.
- [22] Perdew, J. P., Burke, K., & Ernzerhof, M. (1996). Generalized gradient approximation made simple. *Physical Review Letters*, *77*(18), 3865.
- [23] Vanderbilt, D. (1990). Soft self-consistent pseudopotentials in a generalized eigenvalue formalism. *Physical Review B*, *41*(11), 7892.

- [24] Fischer, T. H., & Almlof, J. (1992). General methods for geometry and wave function optimization. *The Journal of Physical Chemistry*, 96(24), 9768-9774.
- [25] Monkhorst, H. J., & Pack, J. D. (1976). Special points for Brillouin-zone integrations. *Physical Review B*, 13(12), 5188.
- [26] Liu, Z. T. Y., Gall, D., & Khare, S. V. (2014). Electronic and bonding analysis of hardness in pyrite-type transition-metal pernitrides. *Physical Review B*, 90(13), 134102.
- [27] Liu, Z. T. Y., Zhou, X., Khare, S. V., & Gall, D. (2013). Structural, mechanical and electronic properties of 3d transition metal nitrides in cubic zincblende, rocksalt and cesium chloride structures: A first-principles investigation. *Journal of Physics: Condensed Matter*, 26(2), 025404.
- [28] Liu, Z. T. Y., Zhou, X., Gall, D., & Khare, S. V. (2014). First-principles investigation of the structural, mechanical and electronic properties of the NbO-structured 3d, 4d and 5d transition metal nitrides. *Computational Materials Science*, 84, 365-373.
- [29] Liu, Q. J., Ran, Z., Liu, F. S., & Liu, Z. T. (2015). Phase transitions and mechanical stability of TiO₂ polymorphs under high pressure. *Journal of Alloys and Compounds*, 100(631), 192-201.
- [30] Baonza, V. G., Cáceres, M., & Núñez, J. (1995). Universal compressibility behavior of dense phases. *Physical Review B*, 51(1), 28.
- [31] Wang, J., Yip, S., Phillpot, S. R., & Wolf, D. (1993). Crystal instabilities at finite strain. *Physical review letters*, 71(25), 4182.
- [32] Qu, D., Li, C., Bao, L., Kong, Z., & Duan, Y. (2020). Structural, electronic, and elastic properties of orthorhombic, hexagonal, and cubic Cu₃Sn intermetallic compounds in Sn–Cu lead-free solder. *Journal of Physics and Chemistry of Solids*, 138, 109253.
- [33] Yalameha, S., Nourbakhsh, Z., & Vashae, D. (2022). ElATools: A tool for analyzing anisotropic elastic properties of the 2D and 3D materials. *Computer Physics Communications*, 271, 108195.
- [34] Voigt, W. (1889). Ueber die Beziehung zwischen den beiden Elasticitätsconstanten isotroper Körper. *Annalen der Physik*, 274(12), 573-587.
- [35] Reuss, A. (1929). Berechnung der Fließgrenze von Mischkristallen auf Grund der Plastizitätsbedingung für Einkristalle. *Zeitschrift Angewandte Mathematik und Mechanik*, 9(1), 49-58.
- [36] Hill, R. (1952). The elastic behaviour of a crystalline aggregate. *Proceedings of the Physical Society. Section A*, 65(5), 349.
- [37] Romain Gaillac, Pluton Pullumbi & François-Xavier Coudert (2016). ELATE: an open-source online application for analysis and visualization of elastic tensors. *J. Phys. Cond. Mat.* 28(27), 275201.
- [38] Frantsevich, I. N., Voronov, F. F., & Bakuta, S. A. (1982). Handbook on elastic constants and moduli of elasticity for metals and nonmetals. *Naukova Dumka*.

- [39] Pugh, S. F. (1954). XCII. Relations between the elastic moduli and the plastic properties of polycrystalline pure metals. *The London, Edinburgh, and Dublin Philosophical Magazine and Journal of Science*, 45(367), 823-843.
- [40] Mai Ye et al. (2023). Strong electron-phonon coupling and enhanced phonon Grüneisen parameters in valence-fluctuating metal EuPd_2Si_2 . *Phys. Rev. B* 107, 195111.
- [41] Md. Maruf Mridha, & Naqib, S. H. (2020). Pressure dependent elastic, electronic, superconducting, and optical properties of ternary barium phosphides (BaM_2P_2 ; $M = \text{Ni}, \text{Rh}$): DFT based insights. *Physica Scripta*, 95, 105809.
- [42] Ravindran, P., Fast, L., Korzhavyi, P. A., Johansson, B., Wills, J., & Eriksson, O. (1998). Density functional theory for calculation of elastic properties of orthorhombic crystals: Application to TiSi_2 . *Journal of Applied Physics*, 84(9), 4891-4904.
- [43] Zhu, S., Zhang, X., Chen, J., Liu, C., Li, D., Yu, H., & Wang, F. (2019). Insight into the elastic, electronic properties, anisotropy in elasticity of manganese borides. *Vacuum*, 165, 118-126.
- [44] Ranganathan, S. I., & Ostoja-Starzewski, M. (2008). Universal elastic anisotropy index. *Physical Review Letters*, 101(5), 055504.
- [45] Parvin, F., & Naqib, S. H. (2021). Pressure dependence of structural, elastic, electronic, thermodynamic, and optical properties of van der Waals-type NaSn_2P_2 pnictide superconductor: Insights from DFT study. *Results in Physics*, 21, 103848.
- [46] Schreiber, E., Anderson, O. L., Soga, N., & Bell, J. F. (1975). Elastic Constants and Their Measurement. *Journal of Applied Mechanics*, 42(3), 747.
- [47] Ali, M. A., Hossain, M. M., Islam, A. K. M. A., & Naqib, S. H. (2021). Ternary boride Hf_3PB_4 : Insights into the physical properties of the hardest possible boride MAX phase. *Journal of Alloys and Compounds*, 857, 158264.
- [48] Rano, B. R., Syed, I. M., & Naqib, S. H. (2020). Ab initio approach to the elastic, electronic, and optical properties of MoTe_2 topological Weyl semimetal. *Journal of Alloys and Compounds*, 829, 154522.
- [49] Teter, D. M. (1998). Computational alchemy: The search for new superhard materials. *MRS Bulletin*, 23(1), 22-27.
- [50] Tian, Y., Xu, B., & Zhao, Z. (2012). Microscopic theory of hardness and design of novel superhard crystals. *International Journal of Refractory Metals and Hard Materials*, 33, 93-106.
- [51] Chen, X. Q., Niu, H., Li, D., & Li, Y. (2011). Modeling hardness of polycrystalline materials and bulk metallic glasses. *Intermetallics*, 19(9), 1275-1281.
- [52] El-Adawy, A., & El-KheshKhany, N. (2006). Effect of rare earth (Pr_2O_3 , Nd_2O_3 , Sm_2O_3 , Eu_2O_3 , Gd_2O_3 and Er_2O_3) on the acoustic properties of glass belonging to bismuth–borate system. *Solid State Communications*, 139(3), 108-113.
- [53] Mazhnik, E., & Oganov, A. R. (2019). A model of hardness and fracture toughness of solids. *Journal of Applied Physics*, 126(12), 125109.

- [54] Anderson, O. L. (1963). A simplified method for calculating the Debye temperature from elastic constants. *Journal of Physics and Chemistry of Solids*, 24(7), 909-917.
- [55] Mahamudujjaman, M., Asif Afzal, M., Islam, R. S., & Naqib, S. H. (2022). First-principles insights into mechanical, optoelectronic, and thermo-physical properties of transition metal dichalcogenides ZrX_2 ($X = S, Se, \text{ and } Te$). *AIP Advances*, 12, 025011.
- [56] Naher, M. I., & Naqib, S. H. (2021). A comprehensive study of the thermophysical and optoelectronic properties of Nb_2P_5 via *ab-initio* technique. *Results in Physics*, 28, 104623.
- [57] Naher, M. I., Mahamudujjaman, M., Tasnim, A., Islam, R. S., & Naqib, S. H. (2022). *Ab-initio* insights into the elastic, bonding, phonon, optoelectronic and thermophysical properties of $SnTaS_2$. *Solid State Sciences*, 131, 106947.
- [58] Naher, M. I., & Naqib, S. H. (2020). Structural, elastic, electronic, bonding, and optical properties of topological $CaSn_3$ semimetal. *Journal of Alloys and Compounds*, 829, 154509.
- [59] Roknuzzaman, M., Hadi, M. A., Abden, M. J., Nasir, M. T., Islam, A. K. M. A., Ali, M. S., Ostrikov, K., & Naqib, S. H. (2016). *Computational Materials Science*, 113, 148 – 153.
- [60] Clarke, D. R. (2003). Materials selection guidelines for low thermal conductivity thermal barrier coatings. *Surface and Coatings Technology*, 163, 67-74.
- [61] Mirzai, A., Ahadi, A., Melin, S., & Olsson, P. A. (2021). First-principle investigation of doping effects on mechanical and thermodynamic properties of Y_2SiO_5 . *Mechanics of Materials*, 154, 103739.
- [62] Fine, M. E., Brown, L. D., & Marcus, H. L. (1984). Elastic constants versus melting temperature in metals. *Scripta Metallurgica*, 18(9), 951-956.
- [63] Naher, M. I., & Naqib, S. H. (2022). First-principles insights into the mechanical, optoelectronic, thermophysical, and lattice dynamical properties of binary topological semimetal $BaGa_2$. *Results in Physics*, 37, 105507.

CRedit author statement

Md. Ashraful Alam: Methodology, Software, Formal analysis, Writing-Original draft. **F. Parvin:** Supervision, Writing-Reviewing and Editing. **S. H. Naqib:** Conceptualization, Supervision, Formal analysis, Writing- Reviewing and Editing.